JOURNAL OF GEOPHYSICAL RESEARCH, VOL. 111, D14301, doi:10.1029/2005JD006479, 2006

Latitudinal and vertical distribution of bromine monoxide in the lower stratosphere from Scanning Imaging Absorption Spectrometer for Atmospheric Chartography limb scattering measurements

C. E. Sioris,[1,2] L. J. Kovalenko,[3] C. A. McLinden,[4] R. J. Salawitch,[5] M. Van Roozendael,[6] F. Goutail,[7] M. Dorf,[8] K. Pfeilsticker,[8] K. Chance,[1] C. von Savigny,[9] X. Liu,[1] T. P. Kurosu,[1] J.-P. Pommereau,[7] H. Bösch,[5] and J. Frerick[10]

Received 13 July 2005; revised 21 March 2006; accepted 24 April 2006; published 19 July 2006.

[1] Vertical profiles of stratospheric bromine monoxide (BrO) in the 15–30 km range are retrieved from SCIAMACHY limb scatter data over the globe. First validation comparisons with the balloon-borne SAOZ-BrO and LPMA/DOAS instruments indicate retrieval biases of ~20% or less. Propagated spectral fitting uncertainties lead to a precision approaching ~25% on a 2 km grid at 25 km. This worsens at higher altitudes because of reduced signal and at lower altitudes because of the reduced penetrability of the atmosphere. In terms of volume mixing ratio (VMR), the single profile precision increases from ~4 pptv at 17 km to ~8 pptv at 27 km. Repeatability, an alternative indicator of precision, is 2–3 pptv for SCIAMACHY retrievals and independent of altitude. The BrO stratospheric number density peak generally lies 5 ± 2 km above the tropopause. In the tropics, the stratospheric BrO VMR generally increases with increasing altitude. The observed stratospheric BrO global distribution is generally consistent with previous balloon measurements but does not agree well with results of a model that uses Br_y inferred only from the observed breakdown of long-lived bromoalkanes (i.e., methyl bromide and halons). We find best agreement with the observed vertical and latitudinal distribution of BrO for model results that include an 8.4 ± 2 pptv contribution to stratospheric Br_y, most of which is expected from the breakdown of VSL (very short lived) bromocarbons, in addition to the ~16 pptv contribution from longer-lived sources. This suggests that stratospheric Br_y exceeds 20 pptv. Profiles of Br_y profiles derived from the balloon measurements of BrO also suggest Br_y is in excess of 20 pptv, but the uncertainty and variability of these results do not allow us to definitively rule out this concentration. We find typical BrO VMRs of ~4 pptv at 15 km in the tropical tropopause layer, suggesting that a significant portion of the bromine from VSL bromoalkane sources may be carried across the tropopause in the form of inorganic decomposition products. We discuss a variety of VSL bromocarbons species that may be contributing to the elevated concentrations of stratospheric BrO.

Citation: Sioris, C. E., et al. (2006), Latitudinal and vertical distribution of bromine monoxide in the lower stratosphere from Scanning Imaging Absorption Spectrometer for Atmospheric Chartography limb scattering measurements, *J. Geophys. Res.*, *111*, D14301, doi:10.1029/2005JD006479.

[1]Harvard-Smithsonian Center for Astrophysics, Cambridge, Massachusetts, USA.
[2]Now at Institute of Space and Atmospheric Studies, University of Saskatchewan, Saskatoon, Saskatchewan, Canada.
[3]Division of Geological and Planetary Sciences, California Institute of Technology, Pasadena, California, USA.
[4]Meteorological Service of Canada, Environment Canada, Toronto, Ontario, Canada.
[5]Jet Propulsion Laboratory, Pasadena, California, USA.
[6]Belgian Institute for Space Aeronomy, Brussels, Belgium.
[7]Service d'Aéronomie, Centre National de la Recherche Scientifique, Verrières-le-Buisson, France.
[8]Institute of Environmental Physics, University of Heidelberg, Heidelberg, Germany.
[9]Institute of Environmental Physics, University of Bremen, Bremen, Germany.
[10]European Space Agency/European Space Research and Technology Centre, Noordwijk, Netherlands.

0148-0227/06/2005JD006479$09.00

1. Introduction

[2] Inorganic bromine catalytic cycles likely dominate ozone loss by halogens in the lower stratosphere at all latitudes. Current models used to estimate ozone loss trends assume that the source of stratospheric inorganic bromine (Br_y) is limited to methyl bromide (CH_3Br) and four halons. Because these source gases are all long-lived, these models assume a vertical distribution of Br_y that is close to zero at the tropopause and slowly increases with altitude, or age of air. Many measurements of BrO [e.g., *Wamsley et al.*, 1998; *Pfeilsticker et al.*, 2000; *Harder et al.*, 2000; *Pundt et al.*, 2002] suggest that the Br_y vertical distribution differs from this standard assumption in that there is more Br_y at the tropopause and lower stratosphere than can be supplied solely by CH_3Br and halons. If this is the case, then given the dominance of the Br_y catalytic cycles in this region, current models may be underestimating ozone loss and the halogen contribution to ozone loss [*Salawitch et al.*, 2005].

[3] Stratospheric concentrations of bromine had not stabilized at the time of the last ozone assessment report, despite international efforts to curtail emissions of bromocarbons such as methyl bromide through the Montreal Protocol and subsequent amendments [*World Meteorological Organization* (*WMO*), 2003]. Observations of the total bromine content of long-lived source species (i.e., methyl bromide and halons) indicate a peak in the troposphere occurred near 1998 [*Montzka et al.*, 2003], which should have been realized in the middle stratosphere about the time of our observations (i.e., 2003). Approximately half of the bromine in the stratosphere is thought to be of anthropogenic origin [*WMO*, 2003; *Pfeilsticker et al.*, 2000].

[4] How much reactive bromine is in the upper troposphere and lowermost stratosphere? This question, to be addressed by observations such as those presented below, will help us determine the role of bromine in the explaining spatial and temporal variations of ozone. In spite of its importance to ozone chemistry and rising stratospheric abundances, observations of the global vertical distribution of the most abundant form of active bromine, namely bromine monoxide (BrO), are sparse.

1.1. Review of Previous Measurements

[5] Balloon-borne solar occultation is the only remote sensing technique that has provided us any degree of global coverage of the vertical distribution of BrO [e.g., *Harder et al.*, 2000; *Pfeilsticker et al.*, 2000; *Pundt et al.*, 2002] prior to the launch of SCIAMACHY. However, southern high and midlatitudes remain unexplored by balloons. This measurement technique generally offers more precise vertical profiles of BrO than are possible from limb scattering because of the high signal-to-noise ratio achievable with the sun as the direct light source and the simpler inversion. The upper altitude is usually limited to the float altitude of the balloon ($\sim$29 km), thus leaving the upper stratospheric BrO profile uncertain.

[6] Balloon-borne measurements of BrO from the DOAS instrument [*Pfeilsticker et al.*, 2000], which began in 1996, are publicly available at http://www.iup.uni-heidelberg.de/institut/forschung/en/groups/atmosphere/stratosphere/data. Another balloon-borne BrO data set, from the SAOZ instrument [*Pundt et al.*, 2002], covers a similar altitude range as the DOAS data, e.g., 15.5–30 km, with the lower limit determined by the impenetrability of the atmosphere due to ozone absorption and Rayleigh extinction as well as a significant contribution from skylight along on the line of sight (LOS) [*Pundt et al.*, 2002]. The SAOZ-BrO data record began in 1997 and has, until now, provided the most profiles of any instrument (15 as of 7 March 2000 and another 8 flights have occurred recently, see http://www.aerov.jussieu.fr/~fgoutail/FlightList.html). Measurements with error bars from SAOZ-BrO will be shown below for coincidences with SCIAMACHY (Scanning Imaging Absorption Spectrometer for Atmospheric Chartography). The error budget of SAOZ-BrO measurements was discussed by *Pundt et al.* [2002]. With the purpose of SCIAMACHY validation, a comparison with BrO from the DOAS instrument is also presented below.

[7] Global coverage of the total column abundance of BrO has been provided by the nadir-viewing Global Ozone Monitoring Experiment (GOME) [e.g., *Chance*, 1998; *Richter et al.*, 2002; *Van Roozendael et al.*, 2002], which also senses BrO remotely by virtue of its near-ultraviolet absorption signature. Comparison of integrated BrO columns from SCIAMACHY limb scattering with GOME total columns will also be presented in this paper.

[8] In situ measurements from aircraft [e.g., *Brune et al.*, 1988] and balloon [*McKinney et al.*, 1997] platforms have also contributed to our record of the vertical and latitudinal distribution of BrO, with the first stratospheric BrO profile recorded in 1987 [*Brune et al.*, 1989]. These measurements are sparse. The in situ technique is still currently being used to measure stratospheric BrO profiles [*Woyke et al.*, 1999].

[9] The mass mixing ratio of total inorganic bromine (including particulate Br) was measured in situ with filter techniques in the 1970s and early 1980s [*Sedlacek et al.*, 1984; *Lazrus et al.*, 1976; *Berg et al.*, 1980; see also *Yung et al.*, 1980]. For example, in the early 1980s, inorganic bromine [Br_y] was determined to be 2.6 pptv at 15 km and 15.6 pptv at an altitude of 25–30 km at 33°N by sensing neutron activation in ^{80}Br with high-resolution gamma spectrometry [*Gallagher*, 1987]. These estimates have a low bias due to a known inefficiency in the collection of BrO and considerable uncertainty in the efficiency for bromine nitrate ($BrONO_2$) [*Gallagher*, 1987]. Unfortunately, these are the two most important inorganic bromine species for the overall stratospheric bromine budget.

1.2. SCIAMACHY Spatial and Spectral Capabilities

[10] Satellite-based limb scattering is the only technique that can currently provide global three-dimensional coverage of BrO on a short timescale [*Sinnhuber et al.*, 2005]. SCIAMACHY [*Bovensmann et al.*, 1999], on board the sun-synchronous Envisat platform, is an 8-channel grating spectrometer that measures scattered sunlight in limb and nadir geometries from 240 to 2380 nm with adequate spectral resolution and signal to noise in channel 2 (320–404 nm) to detect the weak ultraviolet absorption signature of BrO. The full width at half-maximum (FWHM) of the instrumental line shape has been determined to be $\sim$0.20 nm from in-flight data with a robust Fraunhofer line technique [*Caspar and Chance*, 1997]. The photodiode array detector pixels have spectral widths of 0.11 nm, and consequently, SCIAMACHY spectra from channel 2 are undersampled. This undersampling leads to spectral structures in normalized limb radiances as discussed below.

[11] The latitudinal sampling from SCIAMACHY in limb scatter geometry is rather sparse ($\sim$7.5°) because the instrument alternates between limb and nadir viewing under normal operations. The limb swath is 960 km across the orbital track. In the along-track direction, which is the viewing direction in limb scatter mode, the spatial resolution varies inversely with height since the far and nearside radiance contributions from a given layer at a given tangent height (TH) lie further from the tangent point as the layer altitude increases [*Sioris et al.*, 2003]. The standard vertical sampling is 3.3 km. A height of 2.6 km at the tangent point is viewed instantaneously. The theoretical vertical resolution of the BrO profiles is determined by the FWHM of the averaging kernels. It was calculated to be 4 and 5 km at 15 and 30 km, respectively, and a minimum of 3 km at an altitude of 21 km [*Kaiser*, 2001]. The vertical resolution of the retrieved profiles is also discussed in subsection 2.3 below.

1.3. Theoretical Retrieval Precision From Limb Scattering

[12] While an error budget on measured BrO profiles from space-borne and balloon limb scattering measurements has been not compiled previously, simulated retrievals have been performed for both the Optical Spectrograph and Infrared Imager System (OSIRIS) [*Strong et al.*, 2002; *McDade et al.*, 2002] and SCIAMACHY [*Kaiser*, 2001; *Kaiser et al.*, 2002]. Using an optimal estimation scheme, *Kaiser* [2001] found the contribution of the a priori BrO to the retrieval to be less than 50% from 15 to 30 km for BrO using a similar fitting window. A retrieval range of 15–30 km and precisions of 25–50% on a 3 km grid are expected for SCIAMACHY on the basis of the study of *Kaiser et al.* [2002] and *Kaiser* [2001]. At $\sim$12 km, the retrieval precision is estimated to have reached 100% [*Kaiser*, 2001]. The Kaiser *et al.* simulations do not include all of the instrumental effects introduced by SCIAMACHY and thus should be regarded as closer to best case estimates rather than the expected precision and retrieval range. The results of all of these feasibility studies also appear encouraging compared with previous SCIAMACHY sensitivity studies [*Chance et al.*, 1991; *Bovensmann et al.*, 1999], which indicated a theoretical retrieval precision of 50% at best, based only on BrO slant column density (SCD) uncertainties and a typical retrieval range of 20–25 km [*Chance et al.*, 1991] or 20–30 km [*Bovensmann et al.*, 1999].

[13] In this paper we present the pole-to-pole meridional cross section of stratospheric bromine monoxide (15–30 km) from SCIAMACHY and first validation results. In section 2, we describe our method, explore algorithm sensitivities and discuss sources of error. Section 3 shows results and our validation of these results by comparing three vertical profiles of BrO with coincident profiles from balloon-borne instruments. We also compare our results with photochemical model simulations and discuss possible sources of Br_y in the tropical tropopause layer.

2. Method

2.1. Data Analysis

[14] The retrieval algorithm used here is similar to that described previously [*Sioris et al.*, 2003, 2004] for the retrieval of NO_2 profiles from limb scattering. The retrieval consists of two main parts: a spectral fit to obtain SCDs versus tangent height, followed by an inversion of the observed SCDs versus tangent height to number densities versus altitude.

[15] Limb radiances ("level 1 data") are spectrally calibrated and corrected for pixel-to-pixel gain, stray light, etalon signature and dark current using EnviView 2.2.7. To improve the signal-to-noise ratio, spectra recorded at different azimuthal positions during the same elevation step are coadded. The main disadvantage of the azimuthal coaddition is that the across-track spatial resolution reduces to the swath width (i.e., 960 km). Geolocation information for the limb scan such as tangent height, latitude, longitude, solar-observer azimuthal difference angle ($d\phi$), and solar zenith angle (SZA) are also averaged over azimuth. The lower limit of the retrieval range, nominally $\sim$12 km, is based on the knowledge that the Rayleigh optical thickness does not permit probing deeper into the atmosphere. This lower limit is generally fixed because it does not have a significant orbital dependence on any parameter. However, at large SZAs, the lower limit of the retrieval becomes SZA-dependent. Consequently, for SZA $\geq$ 83°, the retrieval can be cut off at 15 km as discussed below.

[16] The Fraunhofer reference is initially the sum of the limb radiance for tangent heights in the 33 to 70 km range. However, tangent heights from the bottom of the reference range (i.e., TH = 33 km) are iteratively removed from the reference coaddition and the retrieval range is extended to this tangent height until the SCD uncertainty at a given tangent height exceeds 100%. This determines the upper altitude of the retrieval. Profile retrieval is attempted only if SCDs obtained from spectra at all selected tangents heights are positive, have uncertainties of <100%, and the spectrum from at least one tangent height has an SCD uncertainty of <50%. At the lower tangent height limit of the high-TH reference ($\sim$33 km typically), there may be a nontrivial BrO signature since $\sim$10% of the total column lies above this height but the gain in BrO precision from extending the reference tangent height range downward outweighs the expected bias. Furthermore, a high tangent height reference is used in the forward model simulations so any bias will likely be taken into account adequately by mimicking the observational technique with the forward model and by assuming an a priori BrO profile shape from a chemical model [see *Strong et al.*, 2002] above the retrieval range.

[17] The fitting of the observed spectra consists of a multiple linear regression using 149 spectral pixels covering the 344.1–360.0 nm range with 6 basis functions and a third-order closure polynomial. This fitting window includes two BrO vibronic bands (4-0, 5-0) and part of a third (6-0) and is nearly identical to the optimal window for GOME BrO [*Chance*, 1998]. Absorption cross sections for NO_2 and O_3 [*Bogumil et al.*, 2003] and BrO [*Wilmouth et al.*, 1999] represent three of the basis functions used in the linear least squares fitting of the observed normalized radiance. The BrO and O_3 absorption cross sections were corrected for the solar I_0 effect [*Aliwell et al.*, 2002] using the 1 cm^{-1} resolution "Chance/Kurucz" solar spectrum [*Berk et al.*, 1999; *Chance and Spurr*, 1997; *Kurucz*, 1995, and references therein] as I_0.

[18] The *Bogumil et al.* [2003] set of NO_2 reference spectra was chosen because it includes a low temperature

(203 K) spectrum that provides significantly better spectral fitting than the *Vandaele et al.* [1998] cross sections in atmospheric regions where the temperature tends to fall below 200 K: the tropical tropopause and the polar vortex. The *Wilmouth et al.* [1999] BrO cross sections are available at only two temperatures: 228 and 298 K. The peak absorption of the 6-0 band, which is included in the fitting window, changes by ~7% between 203 and 223 K [*Fleischmann et al.*, 2004]. Comparing the Wilmouth *et al.* cross sections to those of Fleischmann et al. after convolution of each to the spectral resolution of SCIAMACHY (assuming all slit functions are Gaussian and accounting for the finite resolution of the laboratory reference spectra), reveals that the *Wilmouth et al.* [1999] BrO cross sections at the peaks of 6-0, 5-0, and 4-0 bands are systematically higher. The Wilmouth et al. spectroscopic data also give slightly smaller fitting residuals than any of the *Fleischmann et al.* [2004] spectra fitted with NO_2 and O_3 of the nearest temperature. Thus the 228 K Wilmouth spectrum is always used, in combination with sequential fitting of NO_2 and O_3 pairs at 203 K, 223 K, and 243 K.

[19] The measured BrO SCD profiles and their uncertainties from each of the three temperatures, namely 203, 223, 243 K, are used to obtain an SCD profile linearly interpolated to the climatological temperature [*McLinden et al.*, 2002] of the tangent layer. The measured BrO SCD is weakly dependent on the assumed temperature of O_3 absorption between 203 and 223 K, increasing by ~3% for the 20 K increase in the temperature of the O_3 cross section. However, the BrO SCD increases by ~29% for a 20 K increase in O_3 absorption temperature between 223 and 243 K. This is a ~1.5%/K increase in BrO SCD, indicating the importance of interpolating to the correct stratospheric temperature. The simultaneous fitting of O_3 absorption at two different stratospheric temperatures as suggested for zenith-sky geometry [*Aliwell et al.*, 2002] did not improve absolute uncertainties in BrO SCD.

[20] On the basis of an adjusted r^2 test, only a third-order closure polynomial is required to account for spectrally monotonic phenomena (e.g., Rayleigh scattering). The fitting window was optimized for SCIAMACHY by finding a local minimum in the absolute BrO SCD uncertainty. The BrO SCD profile is not sensitive to slight changes in the fitting window. For example, the shortening of the window by one pixel at the long wavelength end results in a ~0.8% change in BrO SCDs and a ~0.4% increase in SCD uncertainties.

[21] One of the benefits of using a high-altitude reference is that the wavelength registration during the short period of a limb scan (1 min) is very stable. This is a great advantage as compared with using a daily solar irradiance reference as in GOME BrO spectral fitting [e.g., *Chance*, 1998] or a reference spectrum from a smaller solar zenith angle as is commonly employed in ground-based remote sensing of BrO [e.g., *Schofield et al.*, 2004]. However, we have detected slight wavelength shifts as a function of tangent height during a limb scan using a cross-correlation technique (e.g., up to 3% of a pixel or 0.003 nm). These TH-dependent shifts occur because a relatively large vertical range is instantaneously viewed (i.e., 2.6 km) in the presence of a limb radiance profile with changing slope (due primarily to Rayleigh extinction at lower tangent heights). This results in a variation in the illumination across the slit, which manifests itself spectrally as a wavelength shift to a first approximation. The spectral structure induced by these detectable wavelength shifts is highly correlated ($r = 0.8$) to that from "tilt" [*Sioris et al.*, 2003], a spectral artefact that results when normalizing an undersampled highly structured spectrum with another such spectrum of a different slope. Thus, in the data analysis, we use a simulated "tilt" pseudoabsorption spectrum [*Sioris et al.*, 2003] to account for the correlated shift and "tilt" signatures in the normalized radiances. This pseudoabsorber is absolutely critical and is the most important term in the linear regression model besides the offset (0th-order closure term), accounting for sharp features near Fraunhofer lines with optical depths as large as 2% at TH = 11 km. Omitting this pseudoabsorber in a linear least squares regression results in a threefold increase in BrO fitting uncertainties and a noisy BrO SCD profile. The magnitude of the cross-correlation coefficient with each of the other basis functions is <0.11, indicating it is independent of them as expected. The importance of this pseudoabsorber to the spectral fitting is a consequence of spectral undersampling by SCIAMACHY. The "Chance-Kurucz" solar spectrum from MODTRAN4 [*Berk et al.*, 1999] was selected to simulate the tilt spectrum since it appears to give the smallest residuals. The pixel edge wavelengths used to simulate the "tilt" spectrum are derived from the spectral calibration. The "tilt" spectrum was generated using tangent heights of 15 and 56 km [*Sioris et al.*, 2003] and detrended with a quadratic.

[22] A second pseudoabsorber [*Sioris et al.*, 2004], which is a detrended ratio of the spectral radiance at the lowest reference tangent height to the coaddition of all of the other normalizing radiances, is used to account for repeating spectral structures, particularly at higher tangent heights, including those due to imperfect wavelength calibration (i.e., a consequence of undersampling), and other calibrations (e.g., dark current) which are additive in nature and become significant at low light levels. This empirically derived pseudoabsorber has no significant effect on BrO SCDs: it merely improves fitting residuals by up to ~60% at high tangent heights (e.g., TH = 33 km) and has no effect on BrO SCDs or their uncertainties at low tangent heights, where signal levels are high.

[23] The Ring effect cancels out quite well by using a high-altitude reference as seen from the fitting residuals (see below), which are not larger in Fraunhofer line cores. This is consistent with calculations with a Ring effect model [*Sioris*, 2001] at SCIAMACHY resolution in this fitting window, which show that, at TH = 20 km, the maximum residual Ring effect optical depth using a high tangent height reference is expected to be a factor of ~3 smaller than the BrO optical depth at the 5-0 band. Moreover, adding a $1/I_0$ spectrum to account for Ring effect spectral structures does not generally improve the fitting. At 360 nm, the inelastically scattered fraction of the Rayleigh scattered radiance amounts to 3.8% in the continuum when averaged over all scattering angles. The filling in of the BrO absorption features will lead to a comparable underestimate of the true concentration of BrO.

[24] A third pseudoabsorber is used to remove additional systematic residuals which are orthogonal to any other basis function (i.e., absorber, pseudoabsorber, or polynomial

term). This pseudoabsorber is obtained by fitting the spectrum at the tangent height immediately below the lowest tangent height used in the retrieval with all the basis functions named above. The residual from this fit at a low tangent height is then used as a basis function in fitting all of the spectra at tangent heights included in the retrieval range. This approach accounts for considerable spectral structure presumably due to imperfect wavelength shift and "tilt" corrections. An adjustment to the SCD uncertainties is applied to account for the noise from the reference which is implicitly included in this pseudoabsorber. Without this correction, unrealistically small SCD uncertainties would be obtained. This adjustment simply consists of a scaling according to the ratio of the square root of the window-integrated radiance at the tangent height of interest relative to the reference. This third pseudoabsorber has no impact ($\ll$1%) on BrO SCDs. It simply improves uncertainties significantly at the lowest tangent height in the retrieval range, makes no significant difference to uncertainties at high tangent heights and does not change the SCD profiles themselves, indicating that this empirical approach can account for remaining spectral structures that we are unable to currently model explicitly.

[25] The output of the spectral fitting of the observations is a SCD profile with 1σ fitting uncertainties as a function of tangent height. This is the main input into the second stage of the retrieval: the inversion.

[26] Before beginning the inversion, the tangent height offset as well as the presence and height of the clouds must be determined. Relative pointing between elevation steps during a SCIAMACHY limb scan is expected to be very good (0.17 km) (A. Schwab, personal communication, 1999), however the so-called "engineering tangent heights" provided in the level 1 data can be high by $\sim$1 km or more.

[27] Accurate tangent height registration remains one of the largest technical obstacles with the limb scatter technique. As shown in a sensitivity study below, tangent heights need to be determined with an accuracy of <1 km to avoid large errors in the retrieved profile of BrO. Errors in tangent height determination can also lead to errors in the total column because the strong Rayleigh extinction in the ultraviolet causes the retrieval to be nonlinear with respect to a tangent height offset, particularly at low altitudes. In other words, the profile retrieved after a tangent height correction is not simply the profile retrieved without tangent height correction vertically shifted by the tangent height offset. The tangent height offset is defined here as the engineering "knee" tangent height minus the calculated "knee" tangent height [see also *Sioris et al.*, 2003]. The "knee" is defined as the tangent height where the limb radiance reaches a maximum.

[28] The $\sim$305 nm knee [*Sioris et al.*, 2003] has been shown to improve on pointing information provided by current satellite-borne limb scattering instruments [*Sioris et al.*, 2004]. At this wavelength, the knee occurs at $\sim$45 km and is insensitive to many geophysical sources of radiance variability such as clouds, aerosols and surface albedo, since it is a strongly absorbing wavelength dominated by single scattering. Analysis of SCIAMACHY tangent height offsets derived from the $\sim$305 nm knee technique over a sequence of 11 orbits indicates a drift in attitude of $\sim$100 m in tangent height per orbit. This drift in pointing has been traced to errors in the onboard pitch-and-geolocation prediction model of Envisat [*Kaiser et al.*, 2004]. The onboard orbit model is currently updated twice daily with the true satellite coordinates at which time, large discontinuities in pointing occur and the tangent height bias is reduced. "Knee" tangent heights are simulated using the UGAMP 4-D ozone climatology [*Li and Shine*, 1995] which has monthly temporal resolution, $\sim$2 km vertical resolution and 2.5° latitudinal and longitudinal resolution, based on 5-year means (1985–1989). Figure 1 shows the orbital median of the derived tangent height offsets (and the 1-σ variability) for a sequence of orbits. The discontinuity in orbit 2355 coincides with the daily update of the orbit model [*Kaiser et al.*, 2004] over the Caribbean Sea, which improves the pointing accuracy, as confirmed by the $\sim$305 nm knee. This pointing correction is of $\sim$1 km in magnitude.

[29] Since the derived tangent height offsets appear to be quite latitude-independent over an orbit and the aforementioned drift during the dayside of an orbit is typically on the order of <100 m, a median tangent height offset is calculated over the dayside portion of the orbit to reduce random variations in the derived tangent height offset. In the calculation of this median tangent height offset, 2σ outliers are omitted. Note that there are $\sim$20 scans on the day side of each orbit. The major source of error with the "knee" method, namely planetary wave activity, is most apparent in polar winter. This phenomenon typically causes variations in the calculated "knee" height on the order of 1 km during polar winter because of the strong deviation of ozone and air density in the upper stratosphere and lower mesosphere from the climatology assumed in the radiative transfer model. This finding is consistent with the amplitude and global distribution of planetary waves [*Barnett and Labitzke*, 1990]. Tangent height offsets from scans in polar winter conditions are generally excluded from the orbital median by the filtration of outliers. Other error sources (e.g., temperature profile, surface albedo, and cloud errors, ozone temporal variability, spectral and signal limitations, and radiative transfer model inaccuracy) add up in quadrature to only 290 m typically for SCIAMACHY. The median tangent height offset is used to correct pointing in orbits where its magnitude is greater than the standard deviation of the tangent height offsets averaged over the selected range of the orbit. The latter is typically $\sim$300 m.

[30] The cloud top height must be determined before beginning the inversion as well. The retrieval lower altitude limit is set by the cloud top height if the latter is >11 km. To identify cumulonimbus and high cirrus clouds, a limb radiance profile from channel 6 at a nonabsorbing, optically thin wavelength (e.g., 1.236 μm) is used. An example of a cumulonimbus cloud is shown in Figure 2. Currently, if the cloud is below the field of view, no adjustment is made to the forward model since the impact of a bright surface below the FOV is negligible as shown below.

2.2. Inversion

[31] The forward model of the inversion algorithm is fast and accurate. It uses the successive orders of scattering technique in solving the radiative transfer equation [*McLinden et al.*, 2002]. The version of the pseudospherical radiative transfer model (RTM) used in this study was designed specifically for retrievals from limb scatter-

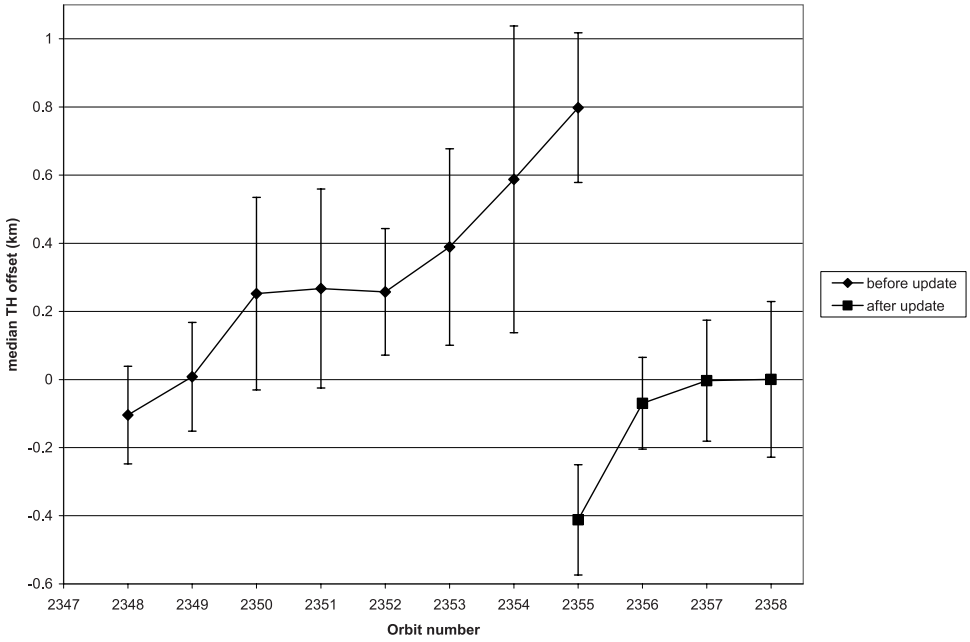

Figure 1. Tangent height offset (engineering-simulated) derived from the ~305 nm knee on 12 August 2002 for a sequence of eleven orbits. Notice the sudden change in the derived tangent height offset during orbit 2355, corresponding to an update of the onboard orbit model.

ing geometry [*McLinden et al.*, 2002]. Additional accuracy can be obtained in a polarized mode where the first 3 elements of the Stokes vector are calculated. The solar zenith angle is varied along the LOS in up to 21 sectors of equal angular size. The temperature dependence of ozone and NO_2 absorption is included, on the basis of the database of model atmospheres contained in the RTM. The vertical distribution of pressure is also key input from the database into the RTM. The database has a latitudinal resolution of 10° and monthly temporal resolution. The assumed O_3 field comes from simultaneous SCIAMACHY measurements [*von Savigny et al.*, 2005a] or from the RTM database if the former is unavailable. The RTM has been modified here to read in updated guesses of the BrO number density profile as generated by the inversion algorithm [*Sioris et al.*, 2003]. In the inversion algorithm, the a priori BrO is only used outside the retrieval range (0–10 km, 32–100 km) and the profile comes from the MISU (Meteorological Institute of Stockholm University) model atmosphere (as shown by *Strong et al.* [2002]). The a priori BrO within the retrieval altitude range is a smoothed version of the BrO number density profile retrieved from the previous limb scan in the orbit. The profile is smoothed so that only the largest local maximum remains. The retrieval is completely insensitive to the a priori BrO in the retrieval range because it is given no weight and is simply used to initialize the first iteration of the forward model simulation. The sensitivity to the a priori BrO profile above and below the retrieval range is quantified below.

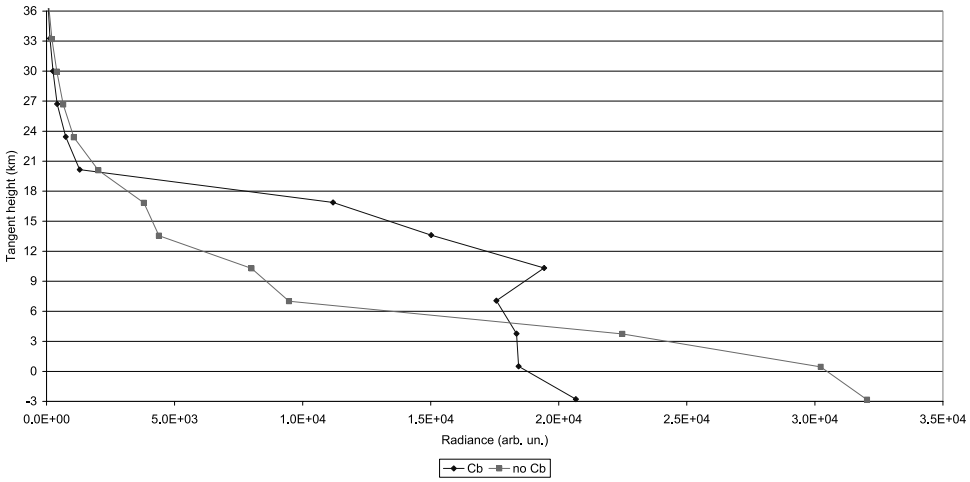

Figure 2. Limb radiance profile at ~1.2 μm observed at 20°S, 38°W in the presence of towering cumulonimbus (Cb) and at 4°N, 44°E (over arid Somalia) in the absence of such clouds on 6 March 2003.

Table 1. Retrieval Sensitivity to Model Simplifications and Geophysical Parameters Used as Model Inputs[a]

Variable	Geometry	Control	Perturbed	Impact on BrO Profile	VCD (>12 km)
Stratospheric aerosol	SZA = 60°, dϕ = 90°	no aerosol	3% strat OD	1–2%	1–2%
O_3	SZA = 54°, dϕ = 59°	Mar 45°N	−10% (uniform)	≤2% (typical)	0.6%
NO_2	SZA = 54°, dϕ = 59°	Mar 45°N	−20% (uniform)	≤0.2% (typical)	<0.2%
Air	SZA = 80°, dϕ = 149°	Mar 75°N	−2% (uniform)	≤2% (typical)	1.6%
BrO above	SZA = 60°, 89°	MISU model	+30% (uniform)	0.1, 0.5% resp.	<0.5%
BrO below	SZA = 33°	MISU model	+2.5e13/cm^2 (tropVCD)[b]	<1%	<1%
Surface albedo	SZA = 45°	18%	28%	<1%	<1%
T-dep	SZA = 80°, dϕ = 149°	231 K	fit w/221 K O_3	13.5% (30 km), 3% (12 km)	5%
T (systematic)	SZA = 59°, dϕ = 64°	Mar 45°N	+3 K	6% (30 km), 2% (12 km)	2%
T (random)	SZA = 59°, dϕ = 64°	Mar 45°N	±3 K	<2%	<2%
Polarization	SZA = 33°, dϕ:50,130°	I, Q, U	I (of Stokes vector)	<0.5% (worst at 12 km)	<0.2%

[a]"T-dep" refers to the use of a coarse (20 K) temperature increment in the cross-section database.
[b]Assumes 1-km thick marine boundary layer containing 1.75×10^8 molec/cm^3 [*Dickerson et al.*, 1999].

[32] The simulated spectra are calculated at tangent heights between 11 and 31 km on a 4-km tangent height grid in the wavelength range 344.1–359.85 nm with steps of 0.21 nm resulting in 76 spectral points. The reference tangent height in the simulations (typically 40 km) is a radiance-weighted average of the tangent heights used in the normalization of the observations. The use of a single reference tangent height speeds up the retrieval slightly.

[33] A cubic is used for closure in the fitting of the modeled normalized spectra. Similar to the treatment of the observations, the spectral fitting of the simulated radiances is performed sequentially with ozone absorption cross sections at 3 temperatures (202, 221, and 241 K). The temperature of O_3 absorption cross section which gives the smallest absolute BrO SCD uncertainty is used to determine the simulated BrO SCD and its uncertainty at a given tangent height. This is almost invariably 221 K. The absorption cross sections of BrO, O_3, and NO_2 that are included in the regression are the same as those used in the forward RTM. The model BrO SCD uncertainties are on the order of 4% and 8% at tangent heights of 11 and 27 km, respectively, for a typical case, and would be considerably larger if fewer wavelengths were simulated.

[34] The number densities at all altitude are simultaneously adjusted on a 2 km grid with a lowest altitude of 11 km and then linearly interpolated onto a 1 km grid for the radiative transfer calculations. This choice of altitude grid size leads to a slightly underdetermined inversion problem since typically 9 pieces of vertical profile information are coming from observed spectra at only 7 different tangent heights. In essence, by choosing a vertical grid of 2 km instead of 3 km, we have traded away some precision to gain a more highly sampled profile. The main purpose of the fine vertical grid is to achieve a better representation of the strong gradient in BrO near the tropopause. The iterative retrieval algorithm is described elsewhere [*Sioris et al.*, 2004]. The second number density guess at altitude z is based on Chahine's method [*Chahine*, 1970]:

$$x_{2,z} = x_{1,z} \Big/ \left[\frac{\left(|z - TH_l| \frac{y_{1,TH_u}}{y_{t,TH_u}} + |z - TH_u| \frac{y_{1,TH_l}}{y_{t,TH_l}} \right)}{(|z - TH_l| + |z - TH_u|)} \right] \quad (1)$$

where TH_l and TH_u are the nearest tangent heights below and above z, respectively. The simulated SCD and observed SCDs are y_i and y_t, with i being the iteration number. Subsequent iterations rely on linear extrapolation or interpolation using the local Jacobian as in equation (3) of the work of *Sioris et al.* [2003]. One tangent height above the retrieval range but below the reference tangent height is simulated (i.e., TH = 31 km). The number densities at altitudes between this tangent height and the reference tangent height (i.e., $31 \leq z < 40$ km) are assumed to be exponentially decreasing according to the atmospheric scale height (i.e., constant mixing ratio). To avoid a discontinuity in the number density at the altitude of the reference tangent height (i.e., z = 40 km), the number density above the reference altitude is also adjusted if necessary, layer by layer starting from the model reference altitude (z = 40 km) and proceeding upward until adjacent 1-km layers are different by more than 10% but less than a factor of 2 (i.e., $1.1 < x_z / x_{z+1} < 2$).

[35] Convergence between measured and modeled SCD profiles is typically reached, using criteria described in the work of *Sioris et al.* [2004], after five iterations or approximately 3 min on a 3 GHz processor. For SZA > 83°, convergence criteria are occasionally not met after nine iterations at the lowest tangent height of the SCD profile, at which point the retrieval is terminated and only considered valid above 15 km.

2.3. Sensitivity Studies and Radiative Transfer Approximations

[36] Numerous sensitivity studies were performed to determine the response of the BrO profile retrieval to a change in the forward model or one of its inputs. After demonstrating the insensitivity of the retrieval to numerous systematic sources of error presented below, numerous simplifications to the forward modeling are justified.

2.3.1. Sensitivity to Geophysical Variables

[37] Many geophysical variables are assumed to be known in our retrieval of BrO. The sensitivity of the inversion to the each of the following variables was quantified: stratospheric aerosol, ozone, NO_2, air, BrO above/below the retrieval range, surface albedo, and temperature. The approach used to account for the temperature dependence of the O_3 and NO_2 absorption was also tested. Results of these sensitivity studies are summarized in Table 1. The highlights of Table 1 are discussed here.

[38] The retrieval of BrO is insensitive to scattering of light by stratospheric aerosols (see Table 1). On the basis of this lack of sensitivity, the BrO retrievals shown throughout

do not include aerosol scattering, thereby saving considerable computational time.

[39] Errors in the ozone concentration lead to errors in BrO concentration because Huggins bands ozone absorption is strong enough to change the effective photon path length in this fitting window. A change in ozone absorption changes the path length in both single and multiple scattering. Because of the significant correlations between BrO and O_3 as a result of photon path length modulation by the latter, the assumed O_3 concentration should be well known. The weak sensitivity of the retrieved BrO vertical column density (VCD) to O_3 is a result of the fact that the BrO peak occurs below the O_3 peak and thus biases in retrieved BrO only occur at altitudes where the BrO number density is relatively small.

[40] The contribution of the a priori BrO above the retrieval range is determined to be of minor significance (<0.5%) even at the top of the retrieval range. This is because the BrO number density immediately above the retrieval range is adjusted during the retrieval, as described above, assuming a constant BrO VMR. This is a key improvement of the retrieval algorithm over previous efforts [*Sioris et al.*, 2003].

[41] The retrieval is extremely insensitive to surface albedo (Λ) and presumably low clouds, as only a small fraction of the total radiance comes from photons that have penetrated down to the surface, reflected and then scattered tangentially in the stratosphere out to space. Furthermore, there is an effective cancellation of this multiple scattering path by normalizing with high tangent heights. The value of Λ is obtained from the wavelength-dependent GOME surface albedo database [*Koelemeijer et al.*, 2003] (incorporated into the RTM) but is fixed to 0.18 for all sensitivity studies in this work.

[42] The temperature dependence of the ozone cross section used in the forward model simulations and in the spectral fitting of the simulated normalized radiances has been tested with a worst case scenario. First, a temperature of 231 K was assumed for ozone absorption in the RTM and "measured SCDs" were calculated in the 11–31 km range by linearly interpolating between the BrO SCDs found with 221 and 241 K O_3 cross sections. Then a standard retrieval was performed (using sequential fitting, with ozone cross section temperatures of 221 and 241 K). The magnitude of this source of error is typically 5% (i.e., half of the error found in this worst case scenario; see Table 1).

2.3.2. Radiative Transfer Approximations

[43] High sun conditions were chosen to test the scalar approximation for a geometry in which multiple scattering is important, and thus the approximation is poorest. We varied $d\phi$ (defined by *McLinden et al.* [2002]) to cover the range observed by SCIAMACHY at SZA = 33°. On the basis of the lack of sensitivity to model calculations including polarization (see Table 1), only the first element of the Stokes vector is modeled.

[44] Double scattering appears to be an adequate approximation, resulting in <1% retrieval errors. The single scattering approximation is clearly inadequate. Five orders of scattering are used for retrievals in this paper.

[45] Refraction of the tangent ray also leads to negligible changes in the retrieved BrO profile. The impact of refraction occurs at the low tangent heights. However, even at TH = 11 km, the BrO SCD changes by <0.5% and by <0.1% for $31 \geq TH > 11$ km. Thus refraction is neglected in the retrievals.

[46] The discretization of the SZA variation along the limb was also tested. For a near worst case scenario for SCIAMACHY looking across the day-night terminator at $d\phi = 28°$, and for tangent-point SZAs of 88 and 89.9°, 15 and 19 different SZAs, respectively, are required to properly model the radiance within the convergence criteria of the retrieval algorithm. For all retrievals presented below, the forward RTM is set to 21 SZAs around the limb.

[47] The long paths viewed in limb scattering geometry are one of the major advantages of this technique. However, when sharp spatial gradients of BrO are observed, the retrieval may have large systematic errors, particularly because a SCIAMACHY limb scan (0–100 km in TH) covers 400 km in the along track direction. For BrO, the latitudinal gradients are much weaker than for O_3 and OClO at the edge of the polar vortex (see section 3.4 for an illustration of observed BrO profiles inside and outside of the vortex). However, diurnal variation can lead to considerable inhomogeneity along the LOS of SCIAMACHY, and along the path of the incoming solar beam for large SZAs. The impact of a diurnal gradient in the BrO field was studied more extensively in a companion paper [*McLinden et al.*, 2006]. That paper contains details on the forward modeling. Here we explore the dependence of the retrieval error on the tangent point SZA. Worst case scenarios occur when SCIAMACHY is looking from the day side into the night, almost perpendicular to the terminator, or vice versa ($d\phi < 30$ or $>150°$). Because of the Envisat local time (LT), $d\phi$ values tend to be different than 90° (e.g., $d\phi = 21°$) at sunrise and thus SCIAMACHY generally looks across the terminator through diurnal gradients. First, a "true" BrO SCD profile was simulated for a worst case scenario with SCIAMACHY looking from the day side into the night almost perpendicular to the terminator (June, 57.5°S, SZA = 89.4° AM, and $d\phi = 21°$ at the tangent point). Then, the retrieval was performed without scaling for the diurnal variation of BrO. Figure 3 illustrates the error due to the neglect of the diurnal gradient during the inversion. The retrieval was repeated for tangent point SZAs of 88, 87, 86, 84, and 82 to investigate the SZA dependence and for a case with SZA = 89.8° AM, $d\phi = 146°$, 1 March, 82.5°S, appropriate for the southernmost scan in the orbit of BrO shown below (see section 3.4). For the March sunrise case, the gradient in BrO is small because there is very little diurnal variation for this date and latitude. Consequently, retrievals errors are <6% at all altitudes (not shown). However, for the June cases, SCIAMACHY detects light that has traversed a much larger range of SZAs and the impact of the neglected diurnal variation is particularly large at the lowest retrieval altitudes (12–17 km), where smaller actinic flux causes the partitioning to shift into other Br_y species (e.g., $BrONO_2$). As a result, the inversion performed neglecting diurnal variation leads to an underestimation of the BrO number density profile for this geometry. During sunrise, the underestimation decreases monotonically as the SZA goes from 88 to 83°. At SZA = 89.4°, the neglected diurnal variation in BrO is somewhat cancelled by the sharp decrease in far (dark) side limb radiance. On the basis of these studies, diurnal variation is included in the inversion

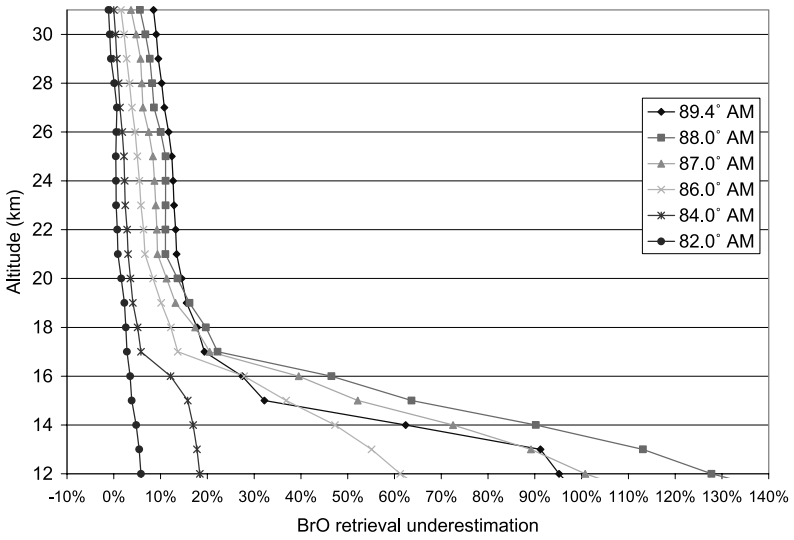

Figure 3. Impact of neglecting diurnal variation during the inversion near sunrise in austral late autumn. Viewing geometries are appropriate to SCIAMACHY for 9 June at 57.5°S. Note that BrO is increasing with decreasing SZA throughout the stratosphere for June 57.5°S during early morning (SZA > 83°).

for tangent point SZAs > 83° so that this source of error is likely to be <10% at all altitudes.

2.3.3. Other Diagnostic Tests

[48] Correlations between adjacent layers were investigated with a noise-free sensitivity study. This study is also useful for a numerical determination of the vertical resolution of the retrieval, which needs to be well known to interpret whether BrO lies in the upper troposphere (UT) or the lower stratosphere (LS) for example, and depends on the retrieval approach so that previous results [e.g., *Kaiser*, 2001] are not entirely applicable. Also revealed from such a study is the shape of the vertical smoothing function, which needs not be symmetrical. We have repeated the method described by *Sioris et al.* [2003]: a layer is perturbed by adding 7×10^6 molec/cm^3 of BrO, then the resulting simulated SCD profile is inverted assuming the unperturbed profile as a first guess. The response of the retrieval is calculated as $A = \partial \hat{x}_z / \partial x$ where $\partial \hat{x}_z$ is the retrieved excess BrO number density at altitude z due to the perturbation and ∂x is the magnitude of the number density perturbation at the perturbed altitude. At 17 km, the point spread of the response has a FWHM of 2.8 km and exhibits wings. At 23 km, the theoretical FWHM of the response is 2.3 km and appears to be triangular; this indicates less vertical smoothing as a result of reduced multiple scattering as one ascends in altitude. The vertical resolution calculated here is generally consistent with the results of *Kaiser* [2001]. On the basis of these calculations, the vertical smoothing of BrO from higher altitudes will be minor at 15 km. However, we note that the retrieval at 17 km tends to overrespond by 10% (i.e., the area under the averaging kernel for 17 km is 1.1 for both SZA = 60 and 35°), in agreement with *Kaiser* [2001], indicating a slight high bias, which we hypothesize is due to the limited and rapidly decreasing sensitivity with decreasing height at ~ 15 km. The vertical integral of the retrieval response at 23 km is 0.993, indicating the retrieval is more robust at this altitude. Weak correlations are expected between adjacent 2-km layers based on the vertical resolution determined in this sensitivity study.

[49] A numerical approach can also be used to show the robustness of the retrieval method. Twenty limb scans were simulated with realistic Gaussian random noise. The noise was determined using the wavelength and tangent height-dependent limb radiance errors provided in the SCIAMACHY level 1 data. Profiles were retrieved using an initial guess that differed by a factor of 2 from the true profile between 11 and 35 km. The arithmetic average of the 20 retrieved profiles is compared with the true profile in Figure 4. The average of the retrievals shows a small positive bias of 4–7%, which is independent of altitude. At 12 km, there appears to be some minor difficulty in retrieving the profile shape. The standard deviation of the retrieved profiles is on the order of 33% and 55% at 15 and 12 km, respectively, and reaches a relative minimum of 18% at 23 km. As shown below, the uncertainties on individual measurements from real SCIAMACHY data are larger than the standard deviations found with this test because of systematic residuals from fitting the spectra.

[50] A 1 km downward shift in the assumed tangent heights was applied to a sample SCD profile observed by SCIAMACHY at 51°S, on 6 March 2003. The resulting BrO number density profile differs from the control case in shape as retrieval nonlinearity due to strong Rayleigh extinction in the lower stratosphere leads to positive errors (37%) in this altitude region that are larger in magnitude than the negative errors (−16.5%) at the top of the profile. Thus the integrated stratospheric VCD shows a positive bias of 4% to a 1 km error in tangent height. The shape of the profile in the lower stratosphere is also not preserved when tangent height registration errors exist.

2.4. Radiometric and Wavelength Calibration Error

[51] Solar and galactic proton hits on photodiode array detectors [see, e.g., *Smith et al.*, 1981] lead to artificial signal which can severely impact the BrO precision if these enhancements in signal are interpreted during the data analysis as being real (i.e., photon-induced). The worst case scenario is when a noise spike due to proton charge transfer

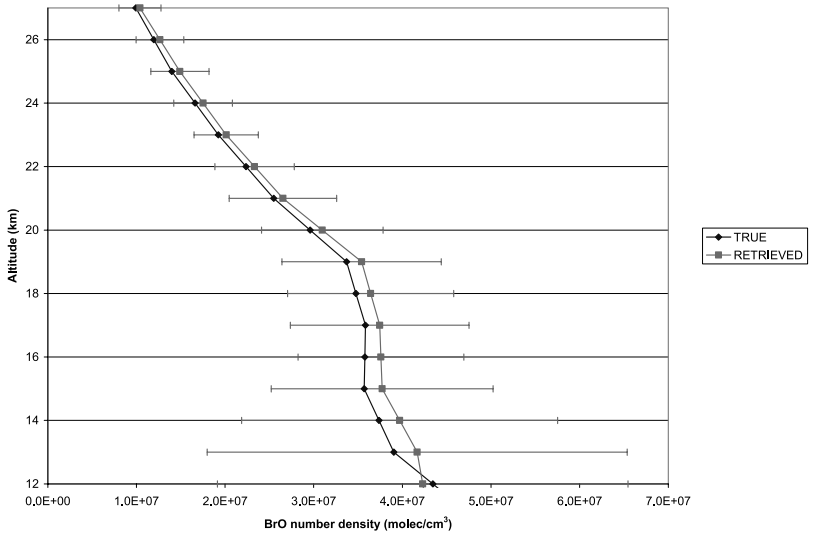

Figure 4. Average of 20 BrO profiles retrieved from synthetic data with realistic Gaussian noise versus the true profile. The error bars show the standard deviation of the retrievals. The initial guess profile is the true profile multiplied by 2.

occurs in a spectrum used for normalization because normalization is applied to all tangent heights of interest and thus the entire limb scan is corrupted in terms of BrO retrieval. To detect the altitude of such events, profiles of ratios of adjacent pixels are used. The ratio of two adjacent pixels is generally altitude-independent up to ~55 km, even at the most strongly absorbing wavelengths in the 344–360 nm region. Above this TH, the ratio profile appears noisy. A radiation hit is flagged if the ratio at that tangent height is $>2\sigma$ different from the mean of the ratio at all tangent heights below ~55 km. This technique has been successfully applied to detect a radiation hit at TH = 46 km to a single pixel that only represented 7% of the total signal of that pixel. This spectrum was removed from the high-TH reference and then the limb scan became scientifically usable with the retrieval scheme described above.

[52] SCIAMACHY has a pronounced spike in its polarization sensitivity at 351.5 nm. This does not cause significant spectral structure because the feature cancels out in the high-TH normalization to a very good approximation because the degree of linear polarization of the atmosphere is TH-independent within ±2% in this window (SZA = 35.9°, $d\phi$ = 66°), similar to results shown by *McLinden et al.* [2002] for 330 nm. Most of the variation is below TH = 22 km where the multiple scattering is more important.

[53] Scattered radiation from outside of the optical axis is rejected well in the ultraviolet. This is confirmed by the linearity of a log linear plot of radiance versus tangent height in the 30–56 km range at a minimal SZA of 35° and in the presence of very bright (as seen from SCIAMACHY limb geometry) cumulonimbus clouds up to 17 km. At 70 km, the off-axis contribution for this worst case scenario is estimated from the limb radiance profile to be <10%. For larger SZAs, the off-axis contribution at TH = 70 km is much smaller (1%) since the contribution from upwelling scattered radiation is smaller. The off-axis contribution in the high-TH reference spectrum is only <0.5% since the radiance between 56 and 70 km composes only 5% of the total.

[54] The noise left after dark current correction is orders of magnitude below the shot noise even at TH = 40 km in the BrO fitting window.

[55] As shown by *Aliwell et al.* [2002], the retrieved BrO abundances are sensitive to wavelength registration errors. There are two types of misalignment: between the measured spectra and the absorption cross sections, and between the Fraunhofer reference (I_0) and the spectra at the tangents heights of interest. The retrieval is not very sensitive (<3% bias) to a typical misalignment of ~0.003 nm relative to the cross sections except at the highest tangent heights (~30 km), where the BrO signature is small and the sensitivity to any error is magnified. The general lack of sensitivity is due to the breadth of the absorption features of BrO and interfering gases, relative to the spectral resolution and sampling of SCIAMACHY. The FWHM of the BrO absorption bands in our fitting window is ~2 nm, which is an order of magnitude larger than either the FWHM of the spectral resolution or the spectral width of a pixel. The fitting of multiple BrO bands also helps minimize this source of error. The second type of misalignment is much more critical (i.e., ~28% bias for a neglected shift of 0.003 nm in I_0 only) but is handled directly by the fitting spectral algorithm, making such errors difficult to quantify but likely of minor importance, judging from the spectral fitting uncertainties (see below).

3. Results and Discussion

3.1. Spectral Fits of the Observations

[56] As shown in Figure 5, it is apparent that the spectral fits are near the shot noise limit but the spectral fitting residuals at different tangent heights still have some common structures. These structures are likely due to imperfect spectral calibration due to undersampling with some minor contribution from inadequate "tilt" correction. This is based on the fact that residual spectral structure lies in the far wings of deep Fraunhofer features (i.e., blends or individual strong lines), which is precisely where these spectral fitting

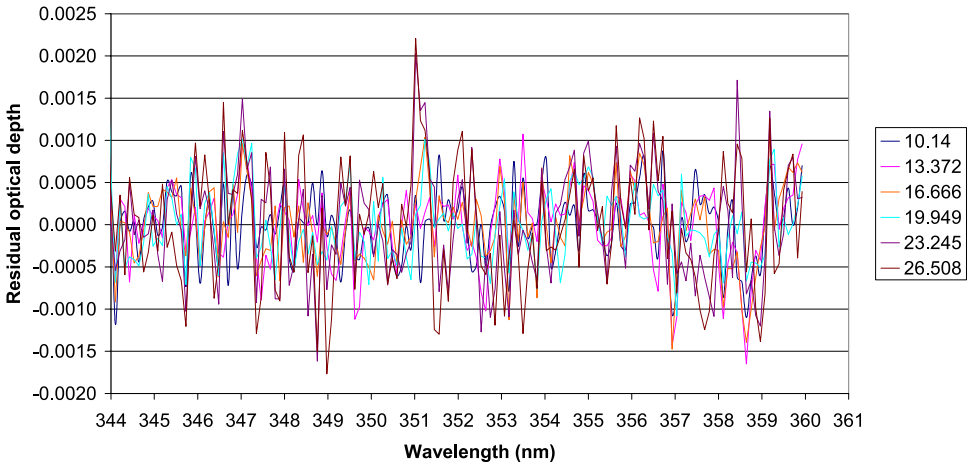

Figure 5. Residual optical depth as a function of tangent height (km) during a sample limb scan. At different tangent heights, the spectral fitting residuals are similar, indicating some unexplained, common source of variance.

error sources leave residual structure. The inadequacy of the "tilt" correction is likely a result of the insufficient quality of available high-resolution exoatmospheric solar irradiance spectra, needed as an input to model this phenomenon. This statement is based on the variability between "tilt" spectra simulated by varying the solar irradiance spectrum used as input.

[57] The common residual signature is not correlated with BrO (see Figure 6a), as the former is more finely structured. Figure 6a shows the BrO absorption differential optical depth at its maximal value during a sample limb scan. Figure 6b shows the O_3 and NO_2 absorption differential optical depth from the same limb scan at the height of the NO_2 SCD maximum (29 km), slightly above the tangent height of the ozone SCD maximum for this fitting window. At the long wavelength end of the fitting window, the differential absorption optical depth in the spectra is predominantly from BrO, especially at low tangent height. In spite of some systematic variance, Figure 6 illustrates that the root-mean-square (rms) of the fitting residuals is small relative to the BrO optical depths from limb scattering.

3.2. Retrieval Precision

[58] Random measurement uncertainties on the number density profile increase rapidly with decreasing altitude in the lower stratosphere because of reduced penetrability due to strong Rayleigh extinction, particularly along the line of sight. This is different from occultation where path lengths are geometric, provided the scattered radiation into the line of sight is minimal relative to the transmitted solar beam. Also, even though the best spectral fits in limb scattering geometry occur at lowest tangent heights, the BrO absorption signature at those tangent heights is coming in large part from above the tangent layer.

[59] In light of the similarity of the spectral fitting residuals at different tangent heights, we believe that repeatability is a more representative measure of the retrieval precision [*McDade et al.*, 2002] than propagation of the spectral fitting uncertainties through the inversion. The repeatability was calculated for a number of latitude bands and generally falls within 2–3 pptv at all heights between 15 and 29 km. The constant VMR repeatability arises because the growing relative variability with decreasing altitude is cancelled by the decreasing mean BrO VMRs with decreasing altitude. As an example, the standard deviation of the profiles for midlatitude autumn and low latitudes are shown in Figure 7 along with the mean vertical distributions of BrO volume mixing ratio in these latitude bands. Precisions calculated from error propagation are shown in the validation section below and are significantly larger (see section 3.3 below) because systematic residuals in the spectral fitting are inevitably propagated into number density uncertainty.

3.3. Validation With Coincident Balloon-Borne Instruments

[60] BrO has a strong diurnal variation at twilight [e.g., *Fish et al.*, 1997]. Because the validating instruments measure near twilight, while SCIAMACHY measures mostly in midmorning, the photochemical model used for the conversion of profiles to the local time of SCIAMACHY, and its inputs, must be accurate. We use a parameterized photochemical model [*Salawitch et al.*, 2002, and references therein] that takes as input the precise latitude and solar declination of the coincidence geolocation as well as measured profiles of temperature, NO_2, BrO, and O_3 as a function of pressure (p). The model calculates the diurnal variation of the Br_y family of species (BrO, BrCl, HOBr, HBr, $BrONO_2$, Br). Model input Br_y and NO_y profiles are adjusted so that calculated BrO and NO_2 at the appropriate local time match the concentrations observed by the balloon-borne instruments (SAOZ-BrO, SAOZ or LPMA/DOAS). Ratios of model BrO at SCIAMACHY local time to the local time of the correlative measurement as a function of altitude are then calculated and used to scale the observed BrO profile from the validating instrument to SCIAMACHY local time. Since the scaling ratio is very sensitive to the measured NO_2 concentration, the use of a locally measured NO_2 profile to constrain the photochemical modeling is particularly important.

[61] For all photochemical model simulations shown in the paper, JPL-2002 chemical kinetics [*Sander et al.*, 2003] are used and the $BrONO_2$ + O reaction is included, using

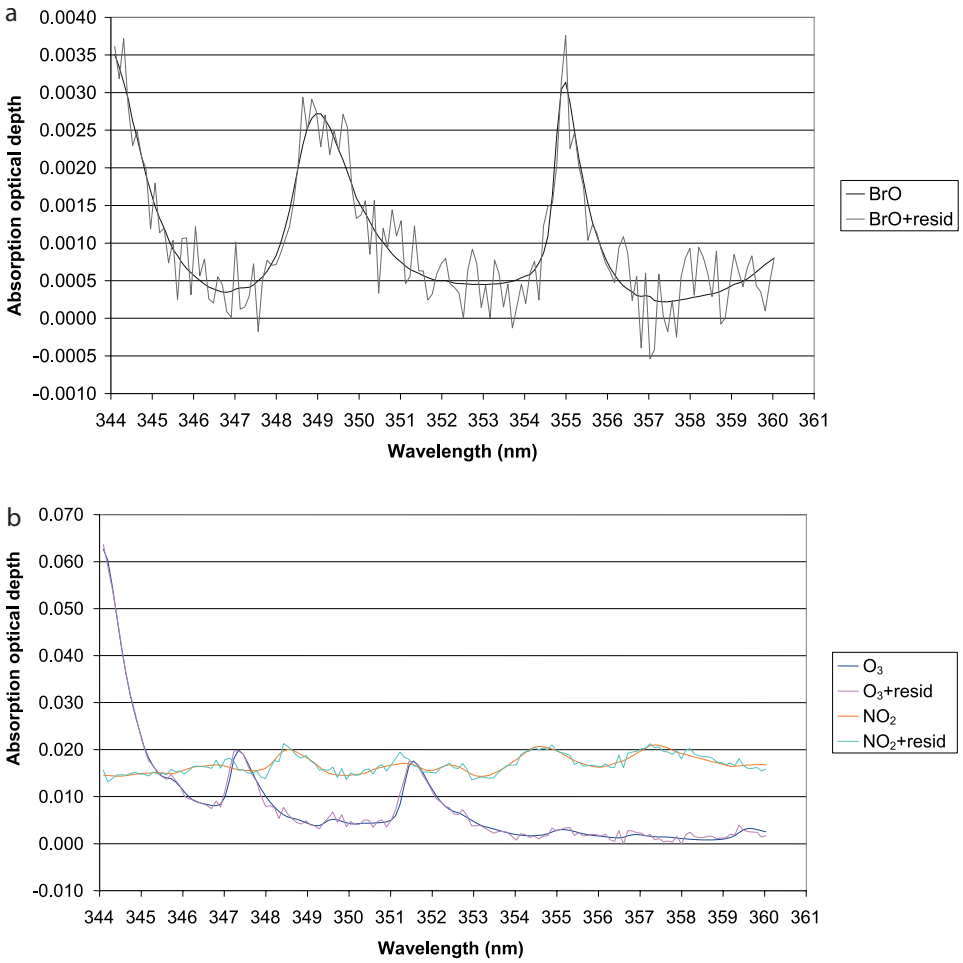

Figure 6. (a) Fitted BrO optical depth spectrum and this spectrum plus spectral fitting residual for TH = 16.7 km on 1 October 2002 at 45°N. The BrO SCD 1-σ precision on this spectrum is 4%, and the RMS of the residuals is 4.1×10^{-4}. (b) Fitted O_3 and NO_2 optical depth spectra and these spectra plus fitting residual for TH = 29.3 km on 1 October 2002 at 45°N.

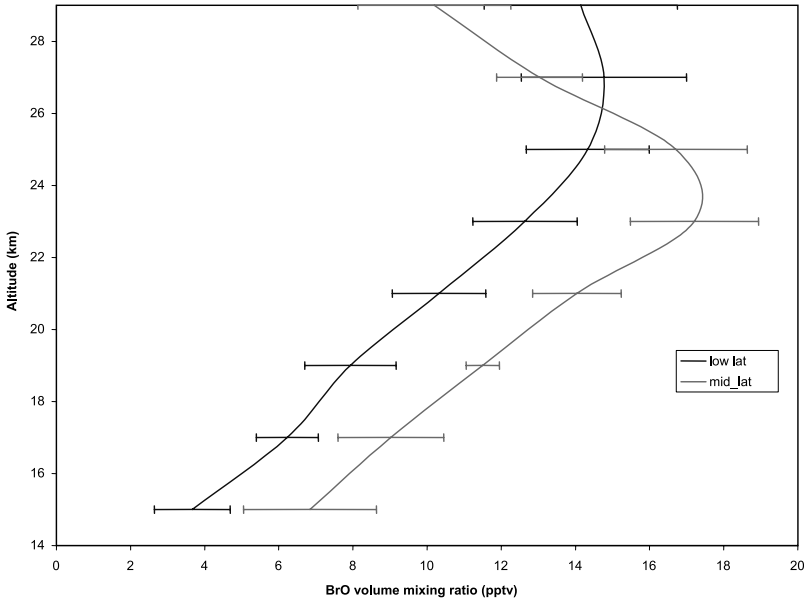

Figure 7. BrO low latitude (20–30°S) and southern midlatitude (36–60°S) mean VMR profiles and their standard deviations, as retrieved from data in early March 2003.

the rate constant measured by *Soller et al.* [2001]. The $BrONO_2$ + O reaction, which is not included in the JPL compendium, increases the calculated BrO/Br_y ratio, particularly above ~24 km [*Sinnhuber et al.*, 2002, 2005]. Estimates of Br_y inferred from measured BrO are therefore reduced, relative to a model based on JPL-2002 kinetics, when this reaction is included. Further details about the model and how it is used to relate measurements of BrO at different times, as well as the effects of $BrONO_2$ + O, are given in Appendix A.

[62] Since the launch of Envisat, the validated SAOZ-BrO balloon-borne instrument has measured two profiles of BrO for which coincident SCIAMACHY data is currently available: one in summer at high latitude and one in autumn over southern France. The DOAS balloon instrument (Heidelberg University) measured a profile at high latitude during the spring of 2003, also coincident with SCIAMACHY.

[63] For each validation case, we have also retrieved a zonal mean BrO for SCIAMACHY. The zonal mean includes all scans from the same calendar day within ±4.0° latitude of the balloon measurement location. The error bar on the zonal mean profile at any altitude is the larger of (1) the propagated spectral fitting errors added in RMS fashion at that altitude or (2) the standard deviation of the zonal observations at that altitude. Approximately 14 scans met these criteria for each validation case.

3.3.1. High-Latitude Summer

[64] The first of the two coincident SAOZ-BrO profile measurements occurred in the late afternoon at Kiruna on 12 August 2002 (see Figure 8a). The SAOZ-BrO instrument was accompanied by the conventional SAOZ instrument, which provides profiles of NO_2 and O_3. BrO slant columns, measured by SAOZ-BrO every 200–300 m during ascent, are smoothed using a triangular filter function (FWMH = 3 km) to improve signal to noise. The same smoothing procedure is applied to BrO SCDs and uncertainties from the midlatitude autumn case (section 3.3.2). Consequently, SAOZ-BrO and SCIAMACHY results should be of approximately the same vertical resolution.

[65] SAOZ-BrO profile error bars include random errors provided by the spectral fit, propagated through the onion peel inversion, and the uncertainty on the residual amount and vertical distribution of BrO above balloon. The latter error source is estimated to be ±2 pptv at the top of the profile, decreasing rapidly at lower altitudes. Systematic errors on the BrO cross section are not included. SAOZ-BrO spectral fits are near the shot noise limit. The evidence for this is two-fold: (1) that spectral fitting residuals appear to be random with largest magnitudes at wavelengths where I_0 is small and (2) resulting retrieval errors are larger when the evening ascent was closer to sunset. The SZA-dependence of the uncertainties accounts for the difference in the magnitude of SAOZ-BrO errors between the two coincidence cases shown here.

[66] For this particular SCIAMACHY BrO profile retrieval, we have replaced the climatological O_3 profile with the coincident SAOZ O_3 to improve the accuracy of the SCIAMACHY BrO retrieval.

[67] We attribute the poorer agreement between the instruments for this flight relative to two other flights (shown below) to a lack of spatial coincidence in the presence of a strong spatial gradient in BrO as evidenced by the GOME total VCD map from that day shown in Figure 8b. The GOME BrO data [*Van Roozendael et al.*, 2002] were binned along-track (e.g., into 320 × 320 km^2 areas on forward scan pixels) to reduce noisiness. The sharp gradient in BrO accounts for most of the difference between the correlative vertical profiles. The average BrO VCD of ground pixels from the nadir viewing GOME with centers lying in the area delimited by the SCIAMACHY across-track swath from the start to the end of the limb scan is $(3.68 \pm 0.68) \times 10^{13}$ molec/cm^2. This agrees well with the VCD above 12 km observed by SCIAMACHY, $(3.37 \pm 1.44) \times 10^{13}$ molec/cm^2, which includes an assumed 4.60×10^{12} molec/cm^2 above the upper altitude of the retrieval (i.e., 29 km). In an equal area encompassing the SAOZ-BrO ascent geolocation, the average GOME BrO VCD was $(3.04 \pm 0.87) \times 10^{13}$ molec/cm^2. SAOZ-BrO observed an integrated VCD of $(2.86 \pm 0.22) \times 10^{13}$ molec/cm^2 above 12 km after diurnal scaling to SCIAMACHY local time and including a 4.0×10^{12} molec/cm^2 BrO VCD above 30 km. The SZAs for the coincident GOME ground pixels were in the 53 to 57° range on that morning, matching the SZA of SCIAMACHY. Thus, within the GOME precision, both profiling instruments agree with GOME on the VCD at this late morning local time at their respective locations. This indicates that the abundance of BrO for this case is primarily stratospheric and the likelihood of a stratospheric gradient between the profiling instruments. The Br_y inferred from constraining the model to SAOZ-measured BrO and NO_2 is also shown in Figure 8a.

3.3.2. Midlatitude Autumn

[68] The second coincidence with SAOZ-BrO (see Figure 9) exemplifies a different latitude and season: midlatitude autumn. Both instruments saw clouds at the tropopause (12 km) near Aire sur l'Adour. Because of the poor vertical sampling and the height instantaneously viewed by SCIAMACHY, 3.3 and 2.6 km, respectively, the altitude range of the retrieval could only be extended down to 17 km to avoid cloud contamination. Using the ~305 nm knee, tangent heights were determined to be offset by +0.61 km. This offset correction was used in the retrieval of SCIAMACHY BrO.

[69] At all 7 SCIAMACHY retrieval altitudes, the zonally averaged SCIAMACHY BrO VMR agrees closely with that of SAOZ-BrO, well within the respective errors of the two profiles. The coincident SCIAMACHY profile also shows good agreement with SAOZ-BrO at most altitudes. The error bars on the single coincident SCIAMACHY profile, calculated by propagating the spectral fitting uncertainties through the inversion, are large as a result of the systematic spectral fitting residuals. The systematic component of the residuals is, by definition, orthogonal to BrO absorption and all other absorbers. The lack of correlation between the systematic residuals and BrO absorption is reinforced here by the validation of SCIAMACHY's accuracy in the 15–29 km range with coincident profiles from accurate balloon-borne sensors.

[70] The observed BrO mixing ratios of this coincidence are larger than those measured for the first coincidence in August, primarily because of the seasonal variation of BrO. As is known from BrO total column measurements and photochemical models, stratospheric BrO is most abundant in winter [e.g., *Sinnhuber et al.*, 2002].

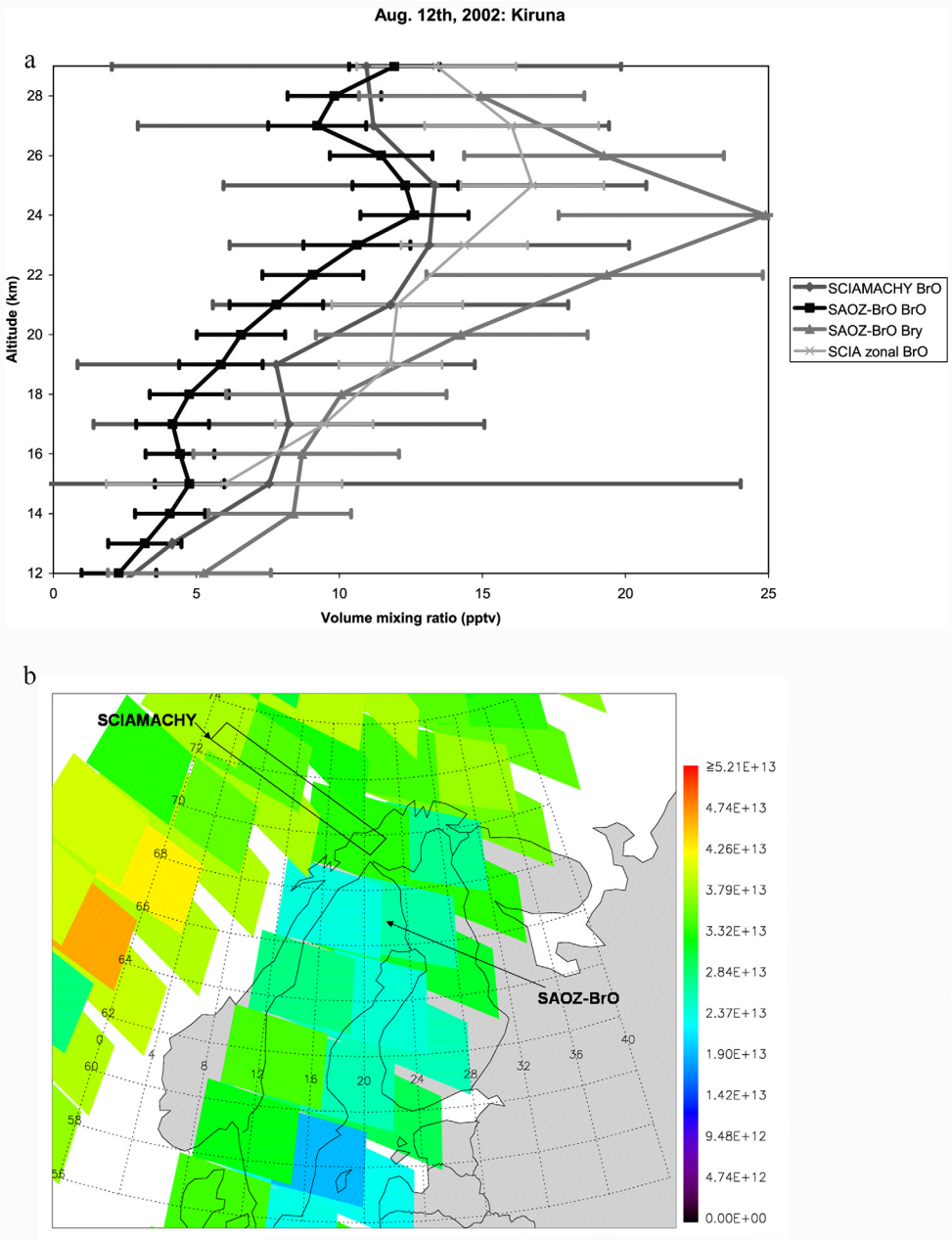

Figure 8. (a) Comparison of BrO profiles measured near Kiruna, Sweden, on 12 August 2002 by SCIAMACHY (71.7°N, 13°E) and SAOZ-BrO (67.7°N, 21.7°E) (see Figure 8b). The SAOZ-BrO profile and error bars, observed during evening ascent, have been scaled to SCIAMACHY local time (~1115 LT, SZA = 57°) using a photochemical model that was constrained by the SAOZ-BrO BrO and SAOZ NO_2 and O_3. The Br_y resulting from this constraint is also shown. The smaller BrO measured by SAOZ-BrO relative to SCIAMACHY may be due to the lack of spatial coincidence of the two measurements in the presence of a BrO gradient, as described in the text. (b) GOME BrO total VCD map of Scandinavia on 12 August 2002 (*Van Roozendael et al.* [2002], version 1.03), indicating a spatial gradient in BrO between the two profiling instruments: SCIAMACHY and the westward looking SAOZ-BrO. Eastern ground pixels of each across-track swath are omitted because they are affected systematically by a known degradation of the GOME scan mirror [*Tanzi et al.*, 2001].

3.3.3. High-Latitude Spring

[71] The LPMA/DOAS coincidence with SCIAMACHY occurred in polar spring conditions (Figure 10). In retrieving this SCIAMACHY BrO profile, we used the collocated and simultaneously observed ozone profile from SCIAMACHY [*von Savigny et al.*, 2005a] and the air number density profile from the DOAS data product.

[72] The typical agreement between SCIAMACHY and the DOAS instrument is ~20%. The high mixing ratios in the lower stratosphere are consistent with the known sea-

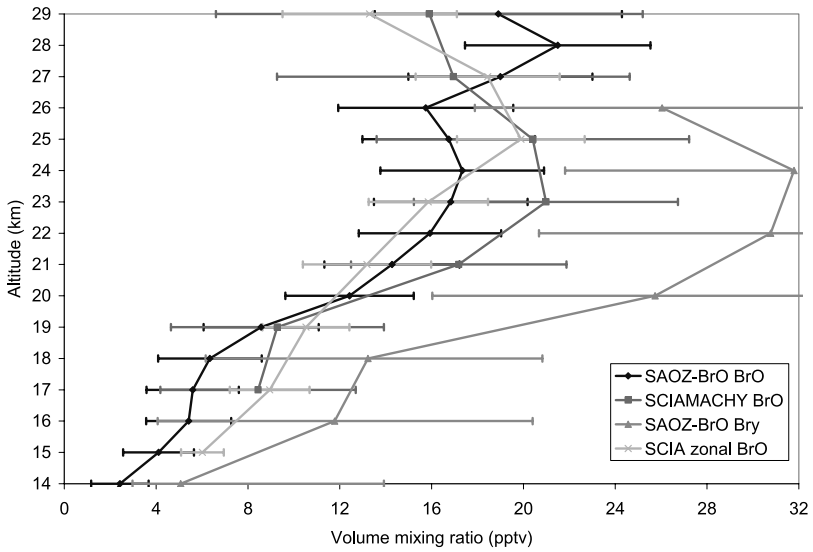

Figure 9. Coincident profiles of BrO from SCIAMACHY (44.7°N, 5°E) and SAOZ-BrO (43.8°N, 0.1°W) on 1 October 2002, near Aire sur l'Adour, France. The SAOZ-BrO BrO profile and its error bars, measured during evening ascent, were scaled to SCIAMACHY local time (~1000 LT, SZA = 51°) using a photochemical model that was constrained by the SAOZ-BrO BrO and SAOZ NO_2 and O_3. The Br_y resulting from this constraint is also shown.

sonal and latitudinal behavior of the BrO vertical profile. Again, the agreement between balloon and satellite based profiles of BrO, which both extend to 15 km altitude, provides confidence that profiles of BrO from SCIAMACHY can be used to test the completeness of the model representation of bromine source species.

3.4. Latitudinal Distribution of BrO

[73] Limb radiance observations from an orbit of SCIAMACHY data on 6 March 2003 were analyzed to investigate the latitudinal and vertical distribution of bromine monoxide (Figure 11). The adjacent orbit (i.e., 5298) of BrO was also retrieved (not shown) to determine whether the orbit shown in Figure 11 is typical of early March 2003. The two orbits exhibit all of the same patterns in the latitude-altitude distribution with very similar ranges of BrO concentrations.

[74] The tropopause height shown in Figure 11 for each profile in this orbit is the daily average from the NCEP reanalysis (http://www.cdc.noaa.gov/cdc/data.ncep.

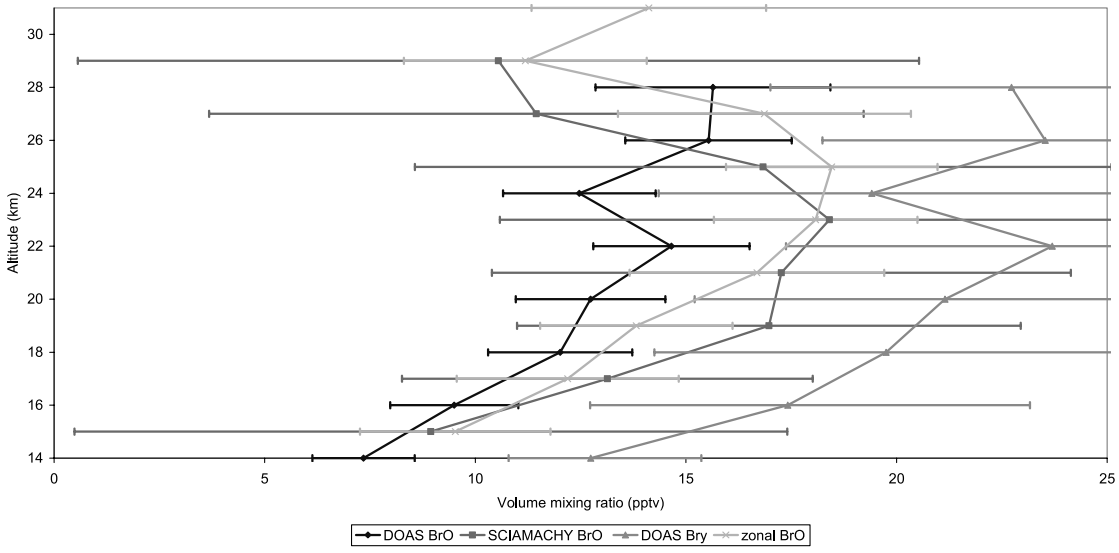

Figure 10. Coincidence between SCIAMACHY (64.5°N, 23.4°E) and LPMA/DOAS (67.9°N, 21.1°E) near Kiruna, Sweden, on 23 March 2003. Profile observed by the balloon-borne DOAS during evening ascent was converted to SCIAMACHY local time (~1100 LT, SZA = 64.4°). Also shown is the Br_y inferred from the DOAS instrument using the method described above assuming a scene albedo of 0.46, on the basis of near-simultaneous satellite-nadir observations.

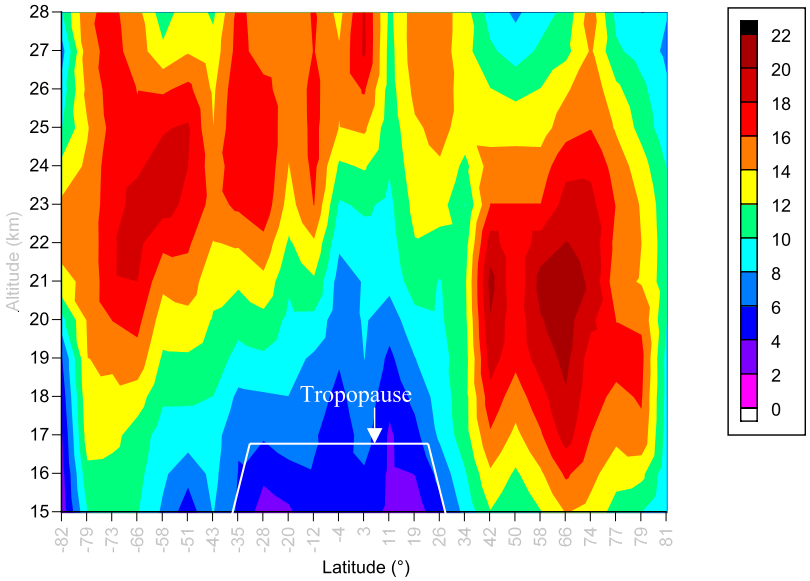

Figure 11. Latitudinal and vertical distribution of BrO volume mixing ratio (pptv) on the morning of 6 March 2003 (orbit 5299). SZAs range from 80° at the northernmost latitude, to a minimum of 35° at the equator and to 89.6° at the southernmost latitude. The BrO mixing ratios in the upper troposphere match the hemispheric asymmetry in tropopause height, indicated with a white line.

reanalysis.html#tropopause) and is appropriate for the latitude and longitude of the limb scan. The BrO mixing ratios depend strongly on tropopause height. For example, at low latitudes, the hemispheric asymmetry in BrO matches quite well with that of tropopause height, suggesting lower values in the upper troposphere than the lower stratosphere, consistent with our understanding of UT/LS BrO [*Pundt et al.*, 2002; *Fitzenberger et al.*, 2000]. This also provides evidence that the retrieval algorithm maintains some sensitivity at these low altitudes.

[75] In terms of number density, the peak altitude is typically at or below 15–17 km at high and midlatitudes. In the tropics, the stratospheric peak altitude rises sharply to 19–23 km, consistent with the model [*McLinden et al.*, 2000] simulations which show a peak at ~22 km and with previous observations of the stratospheric BrO profile at low latitudes [*Pundt et al.*, 2002]. In general, the retrieved BrO number density peak tends to be located 5 ± 2 km above the tropopause and 4–5 km below the stratospheric ozone peak (for unperturbed conditions). Similarly to O_3 [*von Savigny et al.*, 2003] and NO_2 [*Sioris et al.*, 2004], the BrO stratospheric peak in the tropics tends to be much sharper than in the extratropics.

[76] The BrO retrieved from SCIAMACHY (see Figure 11) is consistent with our expectation of the global morphology of this species: (1) The BrO isopleths in the lowermost stratosphere track tropopause height. (2) The rapid diurnal variation of BrO at large SZA near both poles (latitude >76°) is well captured. (3) The altitude of the number density peak at polar latitudes is lower in the Northern Hemisphere than in the Southern Hemisphere in March.

[77] The comparison (Figure 12a) with the nadir-viewing GOME, whose orbit is very similar (descending node of 1030 (LT), lends support to the accuracy of the SCIAMACHY limb scattering measurements. SCIAMACHY VCDs from limb viewing should not and do not exceed GOME total VCDs, since GOME is also sensitive to tropospheric BrO [*Van Roozendael et al.*, 2002]. In Figure 12a, we show the SCIAMACHY partial VCDs of BrO for altitudes above 12, 15, and 17 km, respectively. Although the retrieval uncertainties at these altitudes are expected to be large, a substantial fraction of the total stratospheric column appears to reside below 17 km, particularly at high latitudes, where the stratosphere extends down to ~10 km. When SCIAMACHY BrO profiles are integrated down to 12 km, the absolute agreement with GOME is quite good and is considerably better than the integration of SCIAMACHY profiles down to only 15 km. This suggests that the retrieval generally maintains sensitivity and accuracy down to 12 km, an overall consistency for VCDs of BrO retrieved from GOME and SCIAMACHY, and that a considerable portion of the BrO column in the extratropics lies between 12 and 15 km. In the polar spring region (i.e., northern high latitudes), the GOME BrO VCD is consistently higher than that observed by SCIAMACHY, whereas the VCD difference between the instruments in the polar autumn region (i.e., southern high latitudes) appears smaller. The larger abundance of tropospheric BrO in the springtime as compared to autumn is known from previous GOME observations [e.g., *Chance*, 1998].

[78] Figure 12b compares SCIAMACHY BrO VCD observations (>15 km) to various stratospheric photochemical model simulations [*McLinden et al.*, 2000]. The first model simulation, labeled "org," uses input Br_y measured by the organic bromine method [*Wamsley et al.*, 1998], updated to mid-2003 (see Appendix B). Total stratospheric Br_y for the "org" case equals 20 pptv in the middle and upper stratosphere (Appendix B). The model curves shown in Figure 12b were found using N_2O calculated as described by *McLinden et al.* [2000], latitude-dependent values of the Br_y versus N_2O tracer relation, and are appropriate to the local time of the SCIAMACHY data. Other model BrO

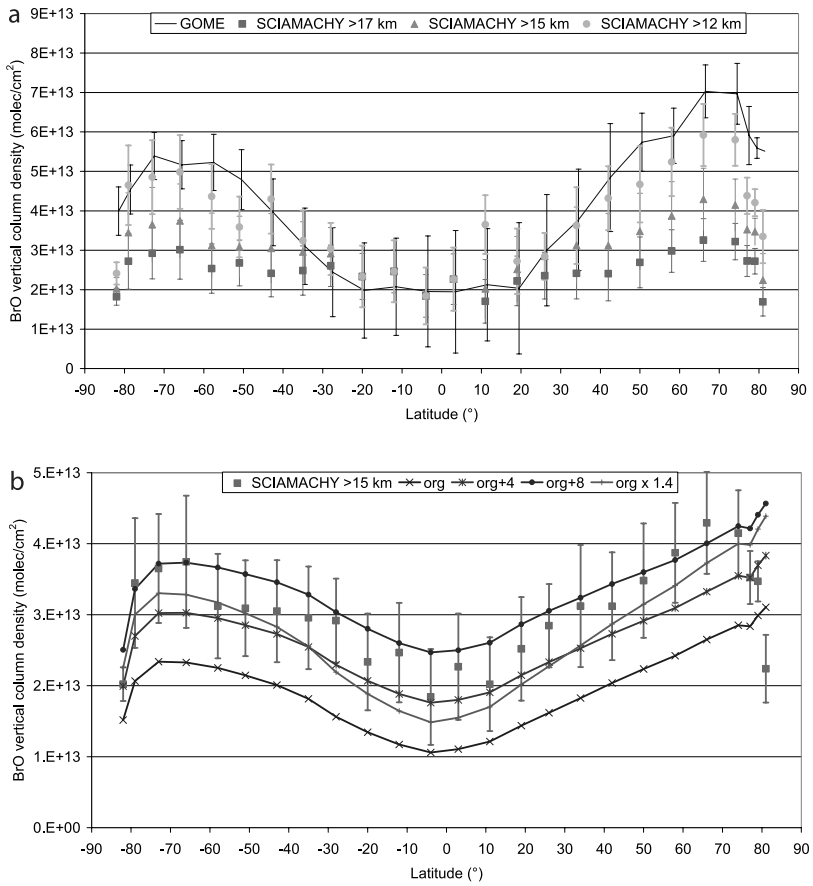

Figure 12. (a) Comparison of BrO vertical columns observed on 6 March 2003 from SCIAMACHY limb scatter and by GOME [*Van Roozendael et al.*, 2002] during coincident orbits. (b) Model [*McLinden et al.*, 2000] BrO columns >15 km using the *Wamsley et al.* [1998] organic Br_y versus tracer relations (updated to March 2003, see Appendix B), and with 4 and 8 pptv Br_y offsets starting at 15 km. The effect of a 41% increase at all altitudes to the organic Br_y profile is labeled "org × 1.4" (see text). These simulations are appropriate to SCIAMACHY local time and latitudinal sampling during orbit 5299.

columns are simulated with Br_y offsets at the tropopause of 4 and 8 pptv applied to the "org" relation between Br_y and N_2O to account, in a simple fashion, for the release of very short lived (VSL) bromoalkanes not measured by *Wamsley et al.* [1998]. This is similar to the approach of *Salawitch et al.* [2005], who added 4 and 8 pptv Br_y offsets at the tropopause to WMO Br_y (i.e., Br_y supplied by methyl bromide and halons only). The only difference between the *Wamsley et al.* [1998] organic Br_y relation used here and the WMO Br_y used by *Salawitch et al.* [2005] is the additional Br_y in the *Wamsley et al.* [1998] profile released by dibromomethane (CH_2Br_2) and bromochloromethane (CH_2BrCl), which amounts to <1 pptv at the tropopause and grows to 2.34 pptv in the middle stratosphere [*Wamsley et al.*, 1998] (see also Table 2). The model columns extend from the lower mesosphere down to 15 km. Model results are used to account for the small partial column in the SCIAMACHY data which lies above the retrieval upper altitude limit (~28 km).

[79] Figure 12b shows good agreement between the stratospheric BrO VCDs measured by SCIAMACHY and the photochemical model simulations only for the cases when Br_y offsets of 4 and 8 pptv are used. The Br_y offset which would best fit the orbit of SCIAMACHY VCDs is 6.1 ± 2 pptv. This was determined by a linear regression of the model column VCDs as a function of Br_y offset. The model curve obtained using the organic tracer relation clearly leads to an underestimation of the stratospheric BrO at all latitudes, primarily because of an underestimation of the mixing ratio of BrO in the lower stratosphere. This comparison indicates that the SCIAMACHY measurements of BrO reported here imply the presence of stratospheric Br_y in excess of ~20 pptv (see Appendix B). The important of "excess bromine in the lowermost stratosphere" is demonstrated by another comparison, that for a model Br_y relation uniformly increased by 41% relative to the "org" curve: e.g., a relation for Br_y versus N_2O similar in shape to the "org" relation, but peaking at 28.8 pptv in the middle and upper stratosphere. Simulations with this large multiplicative increase in Br_y lead to a consistent underestimate of BrO VCD at all latitudes (Figure 12b). This discrepancy reaffirms the notion that a large offset of Br_y (i.e., 6.1 ± 2 pptv) needs to be added to the *Wamsley et al.* [1998] organic Br_y relation, starting near the tropopause, to obtain consistency between modeled and measured BrO VCDs from SCIAMACHY limb scattering. This Br_y offset translates

Table 2. Contribution of Various Hydrobromocarbons to Inorganic Bromine in the TTL and Lowermost Tropical Stratosphere[a]

Bromocarbon	z (Br Activation)	Typical Surface VMR, pptv	Estimated Supply of Br_y, pptv		
			15 km	18 km	τ, days
CH_3Br and halons	UT/LS	$\Sigma \cong 20$	0.5[b]	1.25[c]	>1 year
CH_2Br_2	UT	1.07–1.33[d]	0.25[b]	1.38[c]	120[d]
$CHBr_3$	Free troposphere and UT	1.1–1.83[d,e]	0.75[b]	1.9[b]	26[d]
$CHBr_2Cl$	UT/LS	0.07–0.2[d]	0.09[c]	0.3[c]	69[d]
$CHBrCl_2$	UT/LS	0.17–0.21[d]	0.08[c]	0.13[c]	78[d]
CH_2BrCl	UT/LS	0.07–0.2[d]	0.08[c]	0.17[c]	150[d]
CH_2BrI	Boundary layer	0.2	-	-	0.04[d]
$C_2H_4Br_2$	UT (11–15 km)	0.1[e,f]	0.2	0.2	90[g]
C_2H_5Br	-	0.3[h]	0.19[i]	0.19[i]	60[j]
C_2H_4BrCl	-	0–16	-	-	
C_3H_7Br	UT/LS	0.1–1.0[k]	0.44[l]	0.49[l]	13[d]
C_6H_5Br	-	0–24	0.00	0.00	30[m]
Total			2.57	6.00	
VSL total			2.07	4.75	

[a]See text for details and references. The mean lifetime, τ, is also included. All species listed below are included in the "total" supply whereas "VSL total" includes all species except CH_3Br and halons.
[b]*Dvortsov et al.* [1999], has upper limits of 0.2–0.3 for CH_2Br_2.
[c]*Schauffler et al.* [1999].
[d]*WMO* [2003, and references therein].
[e]Highly variable.
[f]*Sturges* [1993].
[g]*Yung et al.* [1980].
[h]*Low et al.* [2003].
[i]Difference between *Pfeilsticker et al.* [2000] tropopause concentration and *Low et al.* [2003] concentrations in the northern Pacific ocean.
[j]*Donaghy et al.* [1993].
[k]http://www-gte.larc.nasa.gov/gte_mrg1.htm#TRACE-P, 5 min "merges" data from instruments on board P3 and DC-8 aircraft.
[l]Estimate, based on work of *Wuebbles et al.* [2001].
[m]*Atkinson* [1989].

to an 8.4 ± 2 pptv offset relative to an organic Br_y relation defined solely by inputs from CH_3Br and halons.

[80] *Salawitch et al.* [2005] inferred a Br_y profile from SAOZ-BrO balloon measurements down to the tropical tropopause. They found a Br_y offset of >8 pptv to an organic Br_y profile based solely on CH_3Br and halons was needed to bring Br_y profiles from organic and inorganic bromine (balloon BrO) methods into agreement. They also showed that in situ aircraft measurements of BrO were consistent with an offset of ∼7 pptv. The *Salawitch et al.* [2005] simulations were based on the WMO Br_y organic relation, and hence are generally consistent with results presented here. *Pfeilsticker et al.* [2000] also inferred that Br_y from DOAS balloon BrO was ∼5.7 ± 3 pptv higher than Br_y inferred solely from methyl bromide and halons, with the discrepancy extending to the Arctic tropopause. Finally, analyses of ground based BrO profiles by *Schofield et al.* [2004] have suggested a 6 pptv contribution to Br_y from VSL bromocarbons.

[81] An important aspect of the SCIAMACHY observations of BrO, unique to retrievals from this instrument, is the comprehensive sampling of the tropical tropopause layer (TTL). In the TTL, we find a BrO VMR of 4.2 ± 1.4 pptv (1-σ variability, N = 16) at 15.5 km from successive 6 March 2003 orbits over the longitude ranges 34–49°E and 62–73°E, indicating that the BrO VMR and inferred Br_y are significantly greater than zero in this region. This result is in agreement with SAOZ-BrO measurements of BrO obtained from a single balloon flight at 22°S in November 1997 [*Pundt et al.*, 2002; *Salawitch et al.*, 2005]. The highest value was 5 pptv over the Persian Gulf and the minimum was 3 pptv over the Arabian Desert. The origin of the ∼4 pptv of BrO is expected to be partly from uplifted inorganic bromine from the free troposphere [*Ko et al.*, 1997]. Other possible sources are discussed in section 3.5.

[82] Finally, we note that an analysis of the stratospheric bromine budget, based on independent retrievals of BrO from SCIAMACHY limb radiances conducted at the same time as our study, has concluded short-lived source gases supply only 3 ± 3 pptv of Br_y [*Sinnhuber et al.*, 2005]. Our values for the contribution of very short lived bromoalkanes to stratospheric Br_y exceed the *Sinnhuber et al.* [2005] estimate significantly. This difference is due primarily to the fact that the abundance of BrO retrieved from SCIAMACHY radiances using our retrieval algorithm generally exceeds the abundance retrieved by *Sinnhuber et al.* [2005]. The analysis method used by *Sinnhuber et al.* [2005] to infer Br_y from BrO (e.g., model Br_y found from MIPAS measurements of CFC-11 and using a Br_y versus CFC-11 relation from *Wamsley et al.* [1998]; model BrO/Br_y found using a photochemical model constrained by SCIAMACHY NO_2) is similar in concept to the methods used here both to analyze our retrievals of BrO and to scale the balloon-based BrO to the local solar time of SCIAMACHY for purposes of validation (Appendix A). Hence we believe the differing conclusions are driven primarily by differences in retrieved BrO, rather than differences in the techniques used to infer stratospheric Br_y. The most dramatic difference between the BrO retrievals of the two studies is the presence of much higher levels in our study, below ∼18.5 km in the tropics, compared to results shown in Figure 4 (bottom two panels) of *Sinnhuber et al.* [2005]. We believe that part of this

difference stems from their use of a single pointing offset of 1.5 km, which results in longitudinally dependent pointing errors of 500 m or more [*von Savigny et al.*, 2005b], which ultimately lead to possible errors in retrieved lower stratospheric BrO of magnitude $\geq$20% (see Figure 1). As shown above, our retrievals of SCIAMACHY BrO compare favorably to the balloon borne profiles we have used for validation, with rather good agreement between balloon and SCIAMACHY BrO exhibited below 18 km. Clearly validation of SCIAMACHY BrO, particularly in the tropics, would be of great value for understanding the nature of the differences between results reported here and those shown by *Sinnhuber et al.* [2005].

3.5. Possible Sources of Br_y Observed in the Tropical Tropopause Layer

[83] The retrievals of BrO from SCIAMACHY presented above show nonzero levels of BrO in the TTL. The BrO measurements throughout the stratosphere are most consistent with stratospheric total inorganic bromine levels that are $\sim$8 pptv higher than Br_y inferred solely from CH_3Br and halons, with the offset apparent even at the tropopause. The comparison with BrO VCDs from GOME in Figure 12a also supports the notion of the presence of significant concentrations of bromine at the tropical tropopause, especially when one considers that very little BrO (e.g., 0.2 $\pm$ 0.3 pptv [*Schofield et al.*, 2004]) is in the troposphere, far from the ice pack.

[84] In the tropics, observations of the vertical distribution of BrO or Br_y are quite sparse and the Br_y profile near the tropopause is considerably uncertain. Only one balloon flight dedicated to measuring BrO occurred in the tropics in the period predating the launch of Envisat (November 1997 [*Pundt et al.*, 2002]). Some of the in situ BrO measurements reported by *Wamsley et al.* [1998] were also obtained in the tropics. Here, we discuss possible sources of Br_y in the tropical tropopause region that appear to be needed to account for our observations of BrO.

[85] Some Br_y is expected to be transported as BrO from the troposphere [*Ko et al.*, 1997]. The notion of a global, ubiquitous background of tropospheric BrO has received plenty of attention in the past few years, driven by the surprisingly large values of column BrO measured by GOME [e.g., *Chance*, 1998; *Van Roozendael et al.*, 2002]. The source of this BrO could be short-lived biogenic bromoalkanes released from the ocean, such as bromoform ($CHBr_3$) [e.g., *von Glasow et al.*, 2004]. However, the mean value of 0.2 and upper limit of 0.9 pptv for tropospheric BrO reported by *Schofield et al.* [2004] calls into question the ''global nature'' of this background of tropospheric BrO. Nonetheless, it is possible that $\sim$6 pptv of Br_y are present in the tropical upper troposphere [*von Glasow et al.*, 2004], supplied mostly by the local decomposition of $CHBr_3$ and other biogenic bromocarbons released from the tropical ocean and rapidly convected to high altitudes [e.g., *Quack et al.*, 2004; *Salawitch*, 2006]. Values of Br_y of this magnitude [*Salawitch et al.*, 2005, Table 2] are needed to account for balloon-borne measurements of BrO in the tropical tropopause layer at 22°S, obtained during November 1997 [*Pundt et al.*, 2002].

[86] The most abundant very short lived (VSL) bromoalkane is $CHBr_3$. Recent 2-D and 3-D chemical transport model simulations [*Dvortsov et al.*, 1999; *Nielsen and Douglass*, 2001] suggest that the uplifted Br_y from the troposphere amounts to $\sim$1 pptv from bromoform and dibromomethane alone. However, these studies both assumed a 10 day lifetime for removal of inorganic bromine supplied by the decomposition of $CHBr_3$. This assumption does not account for the possibility that heterogeneous reactions might liberate bromine back to the gas phase, following aerosol uptake [*Platt and Hönninger*, 2003]. The recent laboratory study of *Iraci et al.* [2005], demonstrating release of gaseous Br_2 and Br_2O from mixtures of HBr and HOBr exposed to H_2SO_4 solutions, underscores the uncertainty assuming a 10 day lifetime for aerosol washout of the inorganic decomposition products formed following the photochemical loss of $CHBr_3$. In situ observations of bromoform and dibromomethane, their organic and inorganic decomposition products, as well as quantification of the bromine content of aerosols are needed in the tropical upper troposphere to define the stratospheric supply of Br_y from these species.

[87] Other key VSL bromoalkanes include CH_2BrCl, $CHBrCl_2$, $CHBr_2Cl$, C_2H_5Br, $C_2H_4Br_2$, and n-propyl bromide. None of the VSL bromoalkanes are expected to release much of their bromine in the lower troposphere, with the notable exception being bromoform, since photolysis plays a more important role for this species. All of these species are listed by *WMO* [2003], except the C_2-bromoalkanes (ethylene dibromide, ethyl bromide, bromochloroethane) and bromobenzene. The C_2-bromoalkanes also dissociate in the TTL, with photolysis under high sun conditions and reaction with OH being the dominant loss mechanisms (see below). The breakdown of all bromoalkanes (including partial breakdown of longer-lived species such as methyl bromide) in the TTL provides an estimated total of 3 pptv of Br_y, which is approximately the volume mixing ratio of BrO observed there by SCIAMACHY. However, inorganic bromine is known to exist in the boundary layer [e.g., *Dickerson et al.*, 1999] and in the upper troposphere [*Fitzenberger et al.*, 2000] and the source of bromine may not be entirely from the breakdown of brominated organics. For example, a possibly significant global source is the liberation of bromine into the gas phase from sea salt aerosol [e.g., *von Glasow et al.*, 2004].

[88] Table 2 lists the organic sources of bromine at the BrO retrieval lower altitude limit (i.e., 15 km) and in the tropical lowermost stratosphere (i.e., 18 km). At 18 km, the VSL species have released the vast majority of their bromine. Between 18 and 20 km, only another $\sim$0.6 pptv is released, mostly from longer lived CH_2Br_2 and CH_2BrCl (see Table 2), giving a total of 5.3 pptv to be expected from VSL bromocarbon species. Detailed accounting of the associated uncertainties is beyond the scope of this study. For species where model calculations are not available, we estimate the injection of inorganic Br_y into the TTL or lowermost stratosphere from the difference between concentrations in the free troposphere and these altitudes, as observed in the tropics [*Schauffler et al.*, 1999]. For example, this approximation leads to estimates of 0.63 and 0.39 pptv for $CHBr_3$ and CH_2Br_2 in the TTL, which compare well with respect to estimates of 0.5 and 0.25 pptv from model simulations that are available for these species [*Dvortsov et al.*, 1999].

[89] For ethylene dibromide ($C_2H_4Br_2$), there is a lack of recent, published observations. Vertical distribution measurements [e.g., *Rasmussen and Khalil*, 1984] indicate the atmospheric lifetime is sufficiently long for $C_2H_4Br_2$ to reach the stratosphere (see also Table 2). A decreasing trend is expected for this C_2-bromoalkane and its Br_y contribution is expected to be ~0.2 pptv on the basis of observations by *Sturges* [1993] at Barrow, Alaska, in the spring of 1989 of a concentration of 0.1 pptv.

[90] Atmospheric measurements of ethyl bromide (C_2H_5Br) and 1-bromo-2-chloroethane [*Shah and Singh*, 1988] suggest that these VSL C_2-bromoalkanes are weak contributors to stratospheric ozone depletion. The whole air sampler on board the TRIPLE balloon measured [C_2H_5Br] of 0.11 pptv just above the Arctic tropopause (9.5 km) in early 1999 [*Pfeilsticker et al.*, 2000]. Sea level background marine observations [e.g., *Class and Ballschmiter*, 1988; *Carpenter et al.*, 1999] also support the notion that ethyl bromide is likely to be a minor contributor to stratospheric bromine ($\leq$0.2 pptv), partly because it has only one bromine atom per molecule to release. *Donaghy et al.* [1993] calculated an atmospheric lifetime of ~2 months for ethyl bromide, governed by OH.

[91] Bromobenzene (C_6H_5Br) is another highly variable Br_y source gas of note. It is a volatile, short-lived hydrobromocarbon which has been measured in ambient air. *Shah and Singh* [1988] measured median concentrations of 24 pptv at a variety of sites. On the basis of the experimentally measured rate constant for reaction with the hydroxyl radical [*Atkinson*, 1989], the half-life for atmospheric degradation is estimated to be ~1 month. Vertical profiles of this gas have not been measured. Thus the supply of Br_y from this compound is considerably uncertain. We have therefore not considered contributions to Br_y from bromobenzene in Table 2, even though this could be a nontrivial source.

[92] Our estimates of the contribution to Br_y from VSL compounds at 15 and 18 km are 2.07 pptv and 4.75 pptv, respectively (Table 2). Cross tropopause transport of $\leq$4 ppt of inorganic bromine (supplied by the decomposition of VSL bromocarbons near the boundary layer and from sea salt [*Yang et al.*, 2005]) plus the ~4 ppt of Br_y from VSL sources that decompose near the tropopause (see Table 2) results in an estimate for the impact to stratospheric Br_y that is close to the range of our estimate, 8.4 ± 2 pptv, on the basis of the analysis of SCIAMACHY BrO. Note that the BrO/Br_y ratio in the TTL (and other O_3-deficient regions of the troposphere) is ~0.1 to 0.25 [*Yang et al.*, 2005; *von Glasow et al.*, 2004]. Table 2 highlights the possible importance of a suite of bromocarbon compounds and suggests that, combined with cross-tropopause transport of inorganic bromine from nonorganic sources, an 8 ± 2 pptv contribution to stratospheric Br_y from sources other than CH_3Br and halons is plausible.

4. Conclusions and Future Directions

[93] Several sensitivity studies were performed, quantifying the sources of experimental error in retrieving BrO profiles from SCIAMACHY limb radiances. Globally, the largest source of error on the retrieved BrO profile is the shot noise, which dominates the error budget of the integrated vertical column. Inaccurate pointing is the largest source of systematic error. However, using tangent height offsets derived from the "305 nm knee" at low latitudes can minimize this source of systematic error. Although SCIAMACHY "engineering" tangent heights currently lack accuracy, they appear to be precise (i.e., offsets are relatively constant during a half orbit). Taking advantage of the instrument's pointing precision and removing the offsets with "knee" calculations results in tangent heights that are accurate to ~300 m.

[94] In addition, the vertical smoothing of retrieved BrO profiles according to the point spread response function can be considered an additional positive bias, reaching ~10% at 17 km. This may explain some of the differences in the lowermost stratosphere and TTL between SCIAMACHY observations and estimates of BrO from breakdown of organic bromocarbons or in situ BrO observations.

[95] The agreement with the balloon-borne instruments down to 15 km provides confidence that SCIAMACHY is measuring BrO with biases small enough to continue ongoing trend studies, especially considering its unprecedented spatial coverage of this key species. The 2–3 pptv BrO repeatability of SCIAMACHY, based on a zonal repeatability test, also approaches the requirement for such a task. Considering the ozone destroying potential of reactive bromine, the ability to measure such a trend is extremely valuable. The agreement with GOME on the latitudinal distribution of the BrO vertical column combined with the agreement in the Br_y profile with derivations of inorganic Br_y from previous observations of BrO [*Wamsley et al.*, 1998, see Figure 8; *Pfeilsticker et al.*, 2000; *Salawitch et al.*, 2005] confirm the ability of SCIAMACHY to measure the latitudinal distribution of the stratospheric BrO profile. In the tropical tropopause layer, BrO is significantly greater than zero, with likely sources being uplifted inorganic bromine and the release of bromine from the breakdown of very short lived bromoalkanes [*WMO*, 2003]. We find best agreement with the observed vertical and latitudinal distribution of BrO for model results that include an 8.4 ± 2 pptv contribution to stratospheric Br_y from sources other than CH_3Br and halons. The results of *Pfeilsticker et al.* [2000] and *Salawitch et al.* [2005] also suggest a substantial input to stratospheric Br_y from VSL compounds. As noted above, another analysis of the stratospheric bromine budget, based on independent retrievals of BrO from SCIAMACHY limb radiances, concluded short-lived source gases supply only 3 ± 3 pptv of Br_y [*Sinnhuber et al.*, 2005]. Our values for the contribution of very short lived bromoalkanes to stratospheric Br_y exceed the *Sinnhuber et al.* [2005] estimate, because of the fact that the abundance of BrO retrieved using our retrieval algorithm generally exceeds that retrieved by *Sinnhuber et al.* [2005]. More validation work is needed to resolve these differences, particularly in the tropics. However, all of the recent analyses of stratospheric BrO, even that of *Sinnhuber et al.* [2005], conclude that it is unlikely CH_3Br and halons supply the full burden of stratospheric bromine.

[96] Simultaneous measurements of BrO, NO_2, and O_3 in the tropical tropopause region, together with a host of long-lived and VSL bromocarbon species and organic and inorganic intermediates [e.g., *WMO*, 2003], are required to

accurately quantify the particular species responsible for our observations of enhanced levels of stratospheric BrO.

Appendix A: Photochemical Scaling of BrO

[97] A fundamental difficulty that must be overcome in the validation of measurements of BrO from SCIAMACHY is that the space-borne observations of BrO are obtained at a different local time, generally late morning, than the balloon-borne validation observations, typically obtained during twilight for the spectroscopic measurements used here. The mixing ratio of BrO in the low to middle stratosphere exhibits strong diurnal variation, generally peaking close to noon [e.g., *Lary et al.*, 1996]. We use a photochemical box model to scale the balloon-borne observations of BrO to the local time of SCIAMACHY. Assimilation into the model of simultaneous, balloon-borne observations of the abundance of NO_2 is critical to the generation of realistic scaling factors. The uncertainty in photochemically scaled BrO, described below, considers uncertainties in all measured species as well as uncertainties in the kinetic parameters that govern the diurnal variation of BrO.

[98] The photochemical box model has been used previously in many stratospheric studies [e.g., *Salawitch et al.*, 2002, and references therein]. Briefly, the model solves for the abundance of radical (i.e., NO, NO_2, OH, HO_2, ClO, and BrO) and reservoir species (i.e., HNO_3, N_2O_5, HCl, $ClNO_3$, $BrONO_2$, HBr, HOBr, etc.) allowing for diurnal variation and a balance between production and loss of each species integrated over a 24 hour period. The model uses a 15-min time step and an implicit integration scheme. Reaction rates and absorption cross sections are from JPL 2002–25 [*Sander et al.*, 2003]. In addition, for the standard model calculations, we have used the reaction $BrONO_2 + O \rightarrow BrO + NO_3$, with a rate constant of 1.91×10^{-11} exp(215/T), as measured by *Soller et al.* [2001] (this reaction is not listed in the JPL 2002–25 compendium). Input values of temperature, pressure, and ozone used to calculate photolysis rates, for the height range covered by the balloon, are taken directly from the balloon-borne measurements. Data for these quantities, for altitudes outside of this height range, originate from the Middle Atmosphere Program Climatology [*Labitzke et al.*, 1995] and ozonesonde measurements in the troposphere and lower stratosphere [*Dütsch*, 1974], augmented by our own assimilation of in situ observations of ozone, pressure, and temperature in the lower stratosphere and upper troposphere from many ER-2 campaigns (e.g., ASHOE/MEASA). Model inputs for concentrations of radical precursors (i.e., H_2O, CH_4, CO, C_2H_6), and the total abundance of NO_y, Cl_y, and Br_y, are obtained from previously published global simulations by the AER 2D model [*Park et al.*, 1999], with values of Cl_y and Br_y scaled to March 2003 using the tropospheric time series of source species [e.g., *WMO*, 2003]. Values of stratospheric surface area are obtained from the SAGE II climatology of *Thomason et al.* [1997], updated to account for recent observations (L. Thomason, private communication, 2004).

[99] For calculation of the photochemical scaling of BrO, the model is run in a mode where $[Br_y]$ and $[NO_y]$ are treated as adjustable parameters, and are varied such that calculated [BrO] and $[NO_2]$ agree with the balloon-borne observations, at the local measurement time, to within 3%. Since balloon-ascent measurements are used, our model takes into account the change in local time of these measurements with altitude. A sample result, showing measured [BrO] and $[NO_2]$ at 20 km by the SAOZ-BrO and SAOZ instruments, respectively, on 1 October 2002, is shown in Figure A1. The points represent the twilight measurements from SAOZ and the solid line indicates the model results, which pass through the balloon data. The photochemically scaled value of BrO is then the model value of [BrO] for the local measurement time of SCIAMACHY (indicated by the vertical dashed line in Figure A1a). We have examined relations of $[NO_y]$ found from this scaling process versus $[N_2O]$ from the AER model (not shown), and these relations appear reasonable.

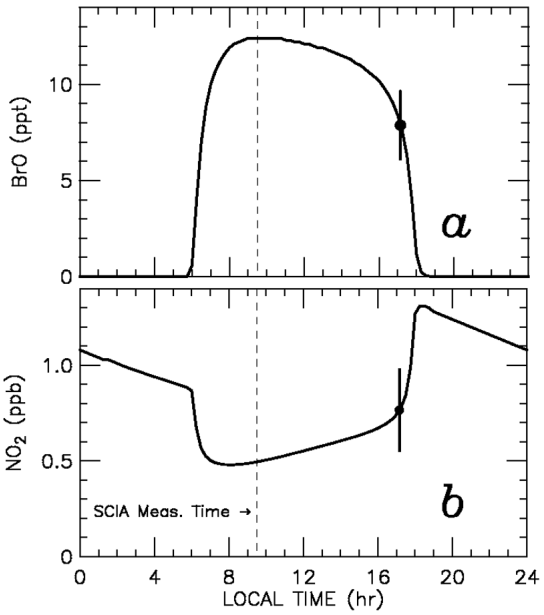

Figure A1. (a) Mixing ratio of BrO measured by balloon-borne SAOZ-BrO instrument at 20 km, 44°N, on 1 October 2002 (data point with error bar) and a photochemical model simulation of BrO, constrained to match measured BrO and NO_2. (b) Same as Figure A1a, except for NO_2 measured by the SAOZ instrument. The vertical dashed line denotes the local time of SCIAMACHY measurements, for the overpass closest in space and time to this balloon flight.

[100] Figure A2a compares the profile of BrO measured by SAOZ-BrO on 1 October 2002 with the photochemically scaled profile (dotted line), which is used for SCIAMACHY validation in the main body of the paper. The error bars on the SAOZ-BrO profile of BrO represent 1σ uncertainty in the measurements, on the basis of considerations such as residuals in the spectral fit. Two error bars are shown for the photochemically scaled profile of BrO in Figure A2a. The inner error bars represent only the uncertainty in the balloon measurements of BrO. The outer error bar combines this uncertainty with the uncertainty in the kinetics used to compute the photochemical scaling factor. Only the outer error bars are shown in the main body of the paper.

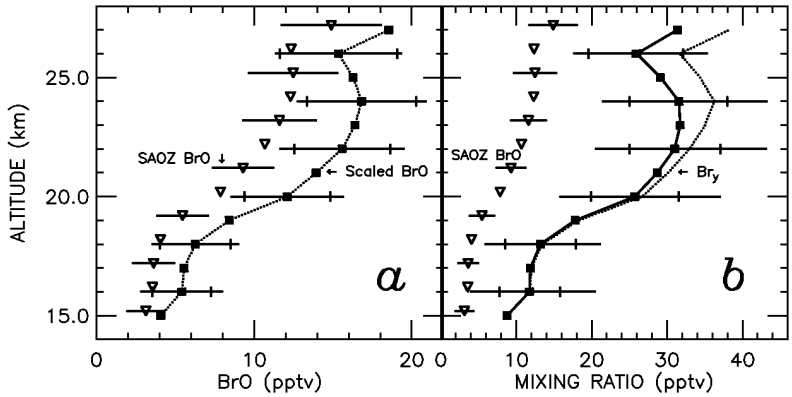

Figure A2. (a) Vertical profile of BrO measured by SAOZ-BrO instrument, 44°N, on 1 October 2002 (upside down triangles with error bars; error bars are shown for every other point, for clarity) and vertical profile of photochemically scaled BrO (boxes; see text). Two error bars are shown for photochemically scaled BrO. The inner error bar represents uncertainty due to measured BrO. The outer error bar represents a combination of the uncertainty due to measured BrO and the uncertainty in the kinetics used to transform BrO from one local time to the local time of the SCIAMACHY observations. For clarity, the SAOZ BrO profile has been offset slightly from the altitude of measurement, which is actually an integer altitude grid. (b) Same as Figure A2a, except a vertical profile of Br_y found using the standard simulation that includes the $BrONO_2$ + O reaction (solid line), resulting from constraining the model to balloon measurements of both BrO and NO_2 is shown, along with the SAOZ-BrO measurement of BrO. Two error bars for Br_y are shown, representing the same uncertainties as described above for photochemically scaled BrO. A profile of Br_y found using JPL 2002–25 kinetics is also shown (dotted line).

[101] We describe first the uncertainty in the kinetic process. The main formation mechanism of BrO is

$$BrONO_2 + h\nu \rightarrow BrO + NO_2, \quad \text{(A1)}$$

characterized by the photolysis frequency J, while loss occurs mainly by the association of BrO and NO_2,

$$BrO + NO_2 + M \rightarrow BrONO_2 + M, \quad \text{(A2)}$$

characterized by the rate constant k. We define the quantity:

$$\Delta(BrO) = BrO(\text{SCIA local time}) - BrO(\text{balloon local time}) \quad \text{(A3)}$$

and compute the uncertainty in Δ(BrO) by adding, in quadrature, the fractional uncertainties in J and k (uncertainties from JPL 2002–25 are used), together with the fractional measurement uncertainty in $[NO_2]$ (reactant in reaction A2). This overall "kinetics uncertainty" is dominated by the 40% uncertainty in J. We have conducted extensive off-line model calculations (not shown) to ascertain that the parameters considered here for the uncertainty estimate of Δ(BrO) are the only parameters that make any significant contribution, provided our basic understanding of the diurnal variation of BrO (e.g., exchange with $BrONO_2$) is correct for the lower and middle stratosphere [see also *Fish et al.*, 1997]. The photochemically scaled profile of BrO is hardly affected by the $BrONO_2$ + O reaction: this reaction has the largest effect on the profile of Br_y that is determined from measured [BrO] and $[NO_2]$, as described below.

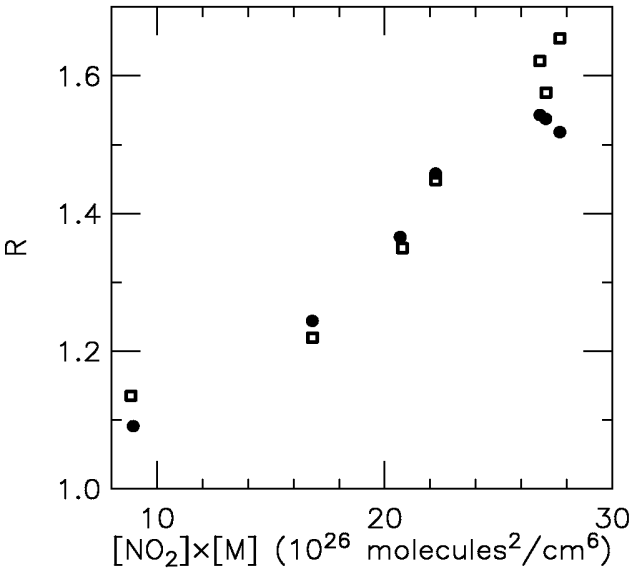

Figure A3. Relation between the ratio of modeled BrO at the time of the SCIAMACHY measurement to modeled BrO at the time of the SAOZ-BrO measurements (denoted "R;" see equation (A5)) versus the product of the number densities of NO_2 and air. The data points correspond to simulations at different altitudes, ranging from 14 to 26 km, for SAOZ data measured on 1 October 2002 at 44°N. The solid circles show model results found using variable local time, as a function of altitude, corresponding to the actual balloon data. The open squares show model results found using fixed local time versus altitude, prescribed as the mean local time of the balloon-borne data.

[102] The overall uncertainty in photochemically scaled BrO, represented by the outer error bar in Figure A2a, is found from:

$$\text{Unc\_Overall} = \text{Unc\_}\Delta(\text{BrO}) + (\text{Unc\_Balloon\_BrO}) \times \text{R} \quad \text{(A4)}$$

where

$$\text{R} = \text{BrO\_at\_SCIA\_observing\_time}/\text{BrO\_at\_balloon\_observing\_time}. \quad \text{(A5)}$$

The quantity R is a model result, representing the computed scaling of [BrO] between the observing time of the balloon and the time of the satellite measurement. We use R to scale the uncertainty in the balloon measurement of BrO, and then add this uncertainty to the uncertainty in Δ(BrO), providing a reasonable estimate of the overall uncertainty in the photochemical scaling of BrO. In general, the overall uncertainty in photochemically scaled BrO is dominated by the uncertainty in the balloon measurement of BrO (inner error bar, Figure A2a).

[103] As noted above, the main body of the paper also shows profiles of [Br_y] that result from constraining the model to balloon measurements of both [BrO] and [NO_2] (see Figure A2b, solid line). The uncertainty of these estimates of [Br_y] was found by performing a sensitivity analysis, varying the kinetic parameters k and J, as well as measured [BrO] and [NO_2], each individually, and then adding in quadrature the resulting fractional changes in computed [Br_y]. Figure A2b shows two error bars for [Br_y]. Again, the inner error bars represent only uncertainties in measured [BrO], while the outer error bar combines this uncertainty with the kinetics uncertainty. As for the case of scaled [BrO], the uncertainty in [Br_y] is dominated by uncertainties in the balloon measurements of [BrO], rather than by uncertainties in k, J, and measured [NO_2]. For altitudes above ~20 km, the profile of [Br_y] found from assimilation of measured [BrO] and [NO_2] using JPL 2002 kinetics (dotted line, Figure A2b) exceeds the value found for the standard simulation (solid line), which includes model representation of the $BrONO_2$ + O reaction. The effect of this reaction is to reduce model values of $BrONO_2$ above 20 km, which raises the BrO/Br_y ratio and therefore reduces the inferred value of Br_y [*Sinnhuber et al.*, 2002, 2005].

[104] We conclude by stressing the importance of accurate knowledge of the product [NO_2] × [M], where [M] represents the density of air, for the computation of scientifically meaningful photochemical scaling factors for BrO. Examination of the reaction kinetics indicates that changes in [BrO] throughout the day are governed by exchange with $BrONO_2$, and hence the photochemical scaling depends on J, k, [NO_2], and [M]. Figure A3 shows the variation of R (equation (A5)) with the quantity [NO_2] × [M], for the SAOZ flight of 1 October 2002 (solid circles). The plot appears to be fairly linear because the ratio J/k is nearly constant with altitude for the observing conditions. Indeed, if we run the model holding local time of BrO and NO_2 measurement constant over the altitude range of the balloon data, rather than letting it vary with altitude, the plot becomes even more linear (open squares in Figure A3) because in this case J/k is nearly independent of altitude.

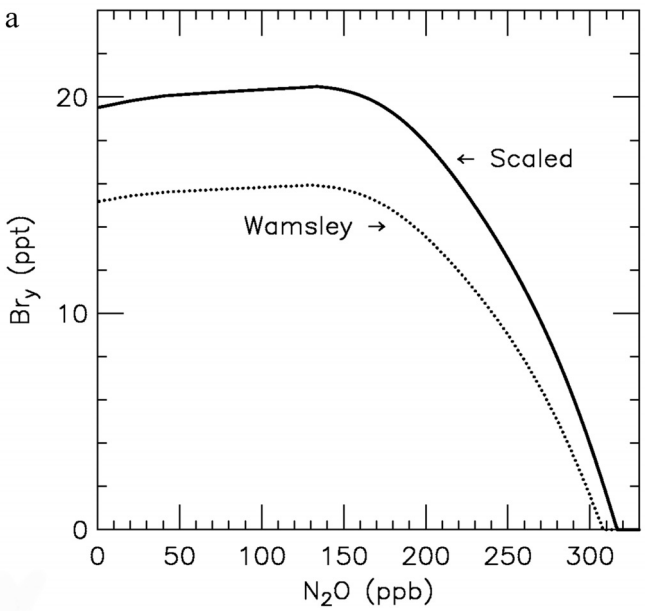

Figure B1. *Wamsley et al.* [1998] organic Br_y relation, based on the measured decomposition of CH_3Br, Halon-1211, Halon-1301, Halon-2402, CH_2Br_2, and CH_2BrCl (dotted line), and updated to mid-2003 (solid line) as described in Appendix B.

[105] Attempts to scale BrO from one time to another using model values for [NO_2] rather than measured values would have additional errors, in direct proportion to the difference between modeled and measured [NO_2]. Figure A3 also indicates the importance of simultaneous measurements of [NO_2], together with [BrO], for validation of satellite observations of [BrO]. Unfortunately, all of the balloon observations of [BrO] obtained for SCIAMACHY validation were not accompanied by measurements of [NO_2], which might limit the overall usefulness of data from these flights for validation purposes.

Appendix B: Temporal Scaling of Bromine Relations

[106] In the paper, comparisons are made between SCIAMACHY retrievals of BrO and model simulations of BrO using a Br_y profile from *Wamsley et al.* [1998] based on measurements of a number of key organic bromine compounds. In this appendix, we describe how the Wamsley organic relation has been scaled for conditions in March, 2003. Figure B1 shows the organic Wamsley relation before and after the temporal scaling.

[107] The estimate of Br_y from the organic method is scaled for "age of air," using the relation between age and N_2O given in Figure 2.12 of *Park et al.* [1999] and a Br_y growth rate of 2.96%/year, calculated from the trend in CH_3Br + halons shown in Figure 1–8 of *WMO* [2003]. This growth is consistent with the results of *Montzka et al.* [2003], who showed that the tropospheric time series of CH_3Br + halons peaked in 1998 (e.g., stratospheric Br_y peaks 3 to 6 years later).

[108] The measurements of BrO from SCIAMACHY and the balloons were all obtained in years 2002 and 2003, nearly a decade after the measurements used to define the *Wamsley et al.* [1998] relations. We have scaled Br_y and N_2O to account for change between these periods on the basis of the following assumptions: (1) growth of Br_y at 2.96%/year (as discussed above) and (2) growth of N_2O at 0.315%/year [*WMO*, 2003, Table 1–12].

[109] **Acknowledgments.** The authors thank Elliot Atlas (NCAR) for propyl bromide measurements during TRACE-P. The work performed at the Harvard-Smithsonian Center for Astrophysics is funded by NASA and the Smithsonian Institution. Research at the Jet Propulsion Laboratory, California Institute of Technology, is performed under contract with NASA. We acknowledge the European Space Agency and the German Aerospace Center for their ongoing cooperation in SCIAMACHY, particularly Sander Slikhuis for valuable insight into the performance of the instrument. We thank the reviewers for helpful comments.

References

Aliwell, S. R., et al. (2002), Analysis of BrO in zenith-sky spectra: An intercomparison exercise for analysis improvement, *J. Geophys. Res.*, *107*(D14), 4199, doi:10.1029/2001JD000329.

Atkinson, R. (1989), *Kinetics and Mechanism of the Gas-Phase Reactions of the Hydroxyl Radical With Organic Compounds*, *J. Phys. Chem. Ref. Data*, *1*.

Barnett, J. J., and K. Labitzke (1990), Climatological distribution of planetary waves in the middle atmosphere, *Adv. Space Res.*, *10*(12), 63–91.

Berg, W. W., P. J. Crutzen, F. E. Grahek, S. N. Gitlin, and W. A. Sedlacek (1980), First measurements of total chlorine and bromine in the lower stratosphere, *Geophys. Res. Lett.*, *7*, 937–940.

Berk, A., G. P. Anderson, P. K. Acharya, J. H. Chetwynd, L. S. Bernstein, E. P. Shettle, M. W. Matthew, and S. M. Adler-Golden (1999), MODTRAN4 user's manual: Software manual, Air Force Res. Lab., Space Vehicles Dir., Air Force Mater. Command, Hanscom Air Force Base, Mass.

Bogumil, K., et al. (2003), Measurements of molecular absorption spectra with the SCIAMACHY pre-flight model: Instrument characterization and reference data for atmospheric remote-sensing in the 230–2380 nm region, *J. Photochem. Photobiol. A*, *157*, 167–184.

Bovensmann, H., J. P. Burrows, M. Buchwitz, J. Frerick, S. Noël, V. V. Rozanov, K. V. Chance, and A. P. H. Goede (1999), SCIAMACHY: Mission objectives and measurement modes, *J. Atmos. Sci.*, *56*, 127–150.

Brune, W. H., D. W. Toohey, J. G. Anderson, W. L. Starr, J. F. Vedder, and E. F. Danielsen (1988), In situ northern mid-latitude observations of ClO, O_3, and BrO in the wintertime lower stratosphere, *Science*, *242*, 558–562.

Brune, W. H., J. G. Anderson, and K. R. Chan (1989), In situ observations of BrO over Antarctica: ER-2 aircraft results from 54°S to 72°S latitude, *J. Geophys. Res.*, *94*, 16,639–16,647.

Carpenter, L. J., W. T. Sturges, S. A. Penkett, P. S. Liss, B. Alicke, K. Hebestreit, and U. Platt (1999), Short-lived alkyl iodides and bromides at Mace Head, Ireland: Links to biogenic sources and halogen oxide production, *J. Geophys. Res.*, *104*, 1679–1689.

Caspar, C., and K. Chance (1997), GOME wavelength calibration using solar and atmospheric spectra, in *Proceedings of the Third ERS Symposium on Space at the Service of our Environment*, edited by T.-D. Guyenne and D. Danesy, *Eur. Space Agency Spec. Publ.*, *ESA SP-414*, 609–614.

Chahine, M. T. (1970), Inverse problems in radiative transfer: Determination of atmospheric parameters, *J. Atmos. Sci.*, *27*, 960–967.

Chance, K. (1998), Analysis of BrO measurements from the Global Ozone Monitoring Experiment, *Geophys. Res. Lett.*, *25*, 3335–3338.

Chance, K. V., and R. J. D. Spurr (1997), Ring effect studies: Rayleigh scattering, including molecular parameters for rotational Raman scattering, and the Fraunhofer spectrum, *Appl. Opt.*, *36*, 5224–5230.

Chance, K. V., J. P. Burrows, and W. Schneider (1991), Retrieval and molecule sensitivity studies for the global ozone monitoring experiment and the scanning imaging absorption spectrometer for atmospheric chartography, *Proc. SPIE Int. Soc. Opt. Eng.*, *1491*, 151–165.

Class, T., and K. Ballschmiter (1988), Chemistry of organic tracers in air, VIII., Sources and distribution of bromo- and bromochloromethanes in marine air and surface of the Atlantic ocean, *J. Atmos. Chem.*, *6*, 35–46.

Dickerson, R. R., K. P. Rhoads, T. P. Carsey, S. J. Oltmans, J. P. Burrows, and P. J. Crutzen (1999), Ozone in the remote marine boundary layer: A possible role for halogens, *J. Geophys. Res.*, *104*, 21,385–21,395.

Donaghy, T., I. Shanahan, M. Hande, and S. Fitzpatrick (1993), Rate constants and atmospheric lifetimes for the reactions of OH radicals and Cl atoms with haloalkanes, *Int. J. Chem. Kinet.*, *25*, 273–284.

Dütsch, H. U. (1974), The ozone distribution in the middle atmosphere, *Can. J. Chem.*, *52*, 1491–1504.

Dvortsov, V. L., M. A. Geller, S. Solomon, S. M. Schauffler, E. L. Atlas, and D. R. Blake (1999), Rethinking reactive halogen budgets in the midlatitude stratosphere, *Geophys. Res. Lett.*, *26*, 1699–1702.

Fish, D. J., S. R. Aliwell, and R. L. Jones (1997), Mid-latitude observations of the seasonal variation of BrO: 2. Interpretation and modelling study, *Geophys. Res. Lett.*, *24*, 1199–1202.

Fitzenberger, R., H. Bösch, C. Camy-Peyret, M. P. Chipperfield, H. Harder, U. Platt, B.-M. Sinnhuber, T. Wagner, and K. Pfeilsticker (2000), First tropospheric profile of BrO, *Geophys. Res. Lett.*, *27*, 2921–2924.

Fleischmann, O. C., M. Hartmann, J. P. Burrows, and J. Orphal (2004), New ultraviolet absorption cross-sections of BrO at atmospheric temperatures measured by time-windowing Fourier transform spectroscopy, *J. Photochem. Photobiol. A*, *168*, 117–132.

Gallagher, C. C. (1987), Inorganic bromine in the lower stratosphere, *J. Atmos. Terr. Phys.*, *49*, 299–302.

Harder, H., H. Bösch, C. Camy-Peyret, M. P. Chipperfield, R. Fitzenberger, S. Payan, D. Perner, U. Platt, B.-M. Sinnhuber, and K. Pfeilsticker (2000), Comparison of measured and modeled stratospheric BrO: Implications for the total amount of stratospheric bromine, *Geophys. Res. Lett.*, *27*, 3695–3698.

Iraci, L. T., R. R. Michelsen, S. F. M. Ashbourn, T. A. Rammer, and D. M. Golden (2005), Uptake of hypobromous acid (HOBr) by aqueous sulfuric acid solutions: Low-temperature solubility and reaction, *Atmos. Chem. Phys. Disc.*, *5*, 1213–1239.

Kaiser, J. W. (2001), Atmospheric parameter retrieval from UV-vis-NIR limb scattering measurements, doctoral dissertation, 228 pp., Univ. of Bremen, Bremen, Germany.

Kaiser, J. W., V. V. Rozanov, and J. P. Burrows (2002), Theoretical precisions for SCIAMACHY limb retrieval, *Adv. Space. Res.*, *29*, 1837–1842.

Kaiser, J. W., et al. (2004), Satellite-pointing retrieval from atmospheric limb-scattering of solar UV-B radiation, *Can. J. Phys.*, *82*, 1041–1052.

Ko, M. K. W., N.-D. Sze, C. J. Scott, and D. K. Weisenstein (1997), On the relation between stratospheric chlorine/bromine loading and short lived source gases, *J. Geophys. Res.*, *102*, 25,507–25,517.

Koelemeijer, R. B. A., J. F. de Haan, and P. Stammes (2003), A database of spectral surface reflectivity in the range 335–772 nm derived from 5.5 years of GOME observations, *J. Geophys. Res.*, *108*(D2), 4070, doi:10.1029/2002JD002429.

Kurucz, R. L. (1995), The solar spectrum: Atlases and line identifications, in *Laboratory and Astronomical High Resolution Spectra*, *Astron. Soc. Pac. Conf. Ser.*, *81*, 17–31.

Labitzke, K., J. J. Barnett, and B. Edwards (1995), Atmospheric structure and its variation in the region 20 to 120 km: Draft of a new reference middle atmosphere, middle atmospheric program (MAP), vol. 16, Univ. of Ill., Urbana, Ill.

Lary, D. J., M. P. Chipperfield, R. Toumi, and T. Lenton (1996), Heterogeneous atmospheric bromine chemistry, *J. Geophys. Res.*, *101*, 1489–1504.

Lazrus, A. L., B. W. Gandrud, R. N. Woodard, and W. A. Sedlacek (1976), Direct measurements of stratospheric chlorine and bromine, *J. Geophys. Res.*, *81*, 1067–1070.

Li, D., and K. P. Shine (1995), A 4-dimensional ozone climatology for UGAMP models, *Internal Rep. 35*, Univ. of Reading, Reading, U. K.

Low, J. C., N. Y. Wang, J. Williams, and R. J. Cicerone (2003), Measurements of ambient atmospheric C_2H_5Cl and other ethyl and methyl halides at coastal California sites and over the Pacific ocean, *J. Geophys. Res.*, *108*(D19), 4608, doi:10.1029/2003JD003620.

McDade, I. C., K. Strong, C. S. Haley, J. Stegman, D. P. Murtagh, and E. J. Llewellyn (2002), A method for recovering stratospheric minor species densities from the Odin/OSIRIS scattered-sunlight measurements, *Can. J. Phys.*, *80*, 395–408.

McKinney, K. A., J. M. Pierson, and D. W. Toohey (1997), A wintertime in situ profile of BrO between 17 and 27 km in the Arctic vortex, *Geophys. Res. Lett.*, *24*, 853–856.

McLinden, C. A., S. C. Olsen, B. J. Hannegan, O. Wild, M. J. Prather, and J. Sundet (2000), Stratospheric ozone in 3-D models: A simple chemistry and the cross-tropopause flux, *J. Geophys. Res.*, *105*, 14,653–14,665.

McLinden, C. A., J. C. McConnell, E. Griffioen, and C. T. McElroy (2002), A vector radiative transfer model for the Odin/OSIRIS project, *Can. J. Phys.*, *80*, 375–393.

McLinden, C. A., C. S. Haley, and C. E. Sioris (2006), Diurnal effects in limb scatter observations, *J. Geophys. Res.*, *111*, D14302, doi:10.1029/2005JD006628.

Montzka, S. A., J. H. Butler, B. D. Hall, D. J. Mondeel, and J. W. Elkins (2003), A decline in tropospheric organic bromine, *Geophys. Res. Lett.*, *30*(15), 1826, doi:10.1029/2003GL017745.

Nielsen, J. E., and A. R. Douglass (2001), A simulation of bromoform's contribution to stratospheric ozone depletion, *J. Geophys. Res.*, *106*, 8089–8100.

Park, J. H., M. K. W. Ko, C. H. Jackman, R. A. Plumb, and K. H. Sage (Eds.) (1999), Models and measurements intercomparison II, *NASA Tech. Memo., NASA TM-1999-209554*.

Pfeilsticker, K., W. T. Sturges, H. Bösch, C. Camy-Peyret, M. P. Chipperfield, A. Engel, R. Fitzenberger, M. Müller, S. Payan, and B.-M. Sinnhuber (2000), Lower stratospheric organic and inorganic bromine budget for the arctic winter 1998/99, *Geophys. Res. Lett.*, *27*, 3305–3308.

Platt, U., and G. Hönninger (2003), The role of halogen species in the troposphere, *Chemosphere*, *52*, 325–338.

Pundt, I., J.-P. Pommereau, M. P. Chipperfield, M. Van Roozendael, and F. Goutail (2002), Climatology of the stratospheric BrO vertical distribution by balloon-borne UV–visible spectrometry, *J. Geophys. Res.*, *107*(D24), 4806, doi:10.1029/2002JD002230.

Quack, B., E. Atlas, G. Petrick, V. Stroud, S. Schauffler, and D. W. R. Wallace (2004), Oceanic bromoform sources for the tropical atmosphere, *Geophys. Res. Lett.*, *31*, L23S05, doi:10.1029/2004GL020597.

Rasmussen, R. A., and M. A. Khalil (1984), Gaseous bromine in the arctic and arctic haze, *Geophys. Res. Lett.*, *11*, 433–436.

Richter, A., F. Wittrock, A. Ladstätter-Weißenmayer, and J. P. Burrows (2002), GOME measurements of stratospheric and tropospheric BrO, *Adv. Space Res.*, *29*(11), 1667–1672.

Salawitch, R. J. (2006), Atmospheric chemistry—Biogenic bromine, *Nature*, *439*, 275–277.

Salawitch, R. J., P. O. Wennberg, G. C. Toon, B. Sen, and J. Blavier (2002), Near IR photolysis of HO_2NO_2: Implications for HO_x, *Geophys. Res. Lett.*, *29*(16), 1762, doi:10.1029/2002GL015006.

Salawitch, R. J., D. K. Weisenstein, L. J. Kovalenko, C. E. Sioris, P. O. Wennberg, K. Chance, M. K. W. Ko, and C. A. McLinden (2005), Sensitivity of ozone to bromine in the lower stratosphere, *Geophys. Res. Lett.*, *32*, L05811, doi:10.1029/2004GL021504.

Sander, S. P., et al. (2003), Chemical kinetics and photochemical data for use in atmospheric studies, *Eval. 14, JPL Publ. 02-25*, Jet Propul. Lab., Pasadena, Calif.

Schauffler, S. M., E. L. Atlas, D. R. Blake, F. Flocke, R. A. Lueb, J. M. Lee-Taylor, V. Stroud, and W. Travnicek (1999), Distributions of brominated organic compounds in the troposphere and lower stratosphere, *J. Geophys. Res.*, *104*, 21,513–21,535.

Schofield, R., K. Kreher, B. J. Connor, P. V. Johnston, A. Thomas, D. Shooter, M. P. Chipperfield, C. D. Rodgers, and G. H. Mount (2004), Retrieved tropospheric and stratospheric BrO columns over Lauder, New Zealand, *J. Geophys. Res.*, *109*, D14304, doi:10.1029/2003JD004463.

Sedlacek, W. A., A. L. Lazrus, and B. W. Gandrud (1984), Measurements of stratospheric bromine, *J. Geophys. Res.*, *89*, 4821–4825.

Shah, J. J., and H. B. Singh (1988), Distribution of volatile organic chemicals in outdoor and indoor air: A national VOCs data base, *Environ. Sci. Technol.*, *22*, 1381–1388.

Sinnhuber, B. M., et al. (2002), Comparison of measurements and model calculations of stratospheric bromine, *J. Geophys. Res.*, *107*(D19), 4398, doi:10.1029/2001JD000940.

Sinnhuber, B. M., et al. (2005), Global observations of stratospheric bromine monoxide from SCIAMACHY, *Geophys. Res. Lett.*, *32*, L20810, doi:10.1029/2005GL023839.

Sioris, C. E. (2001), The filling in of absorption lines in sky spectra due to rotational Raman scattering, Ph.D. thesis, 135 pp., York Univ., Toronto, Ont., Canada.

Sioris, C. E., et al. (2003), Stratospheric profiles of nitrogen dioxide observed by Optical Spectrograph and Infrared Imager System on the Odin satellite, *J. Geophys. Res.*, *108*(D7), 4215, doi:10.1029/2002JD002672.

Sioris, C. E., T. P. Kurosu, R. V. Martin, and K. Chance (2004), Stratospheric and tropospheric NO_2 observed by SCIAMACHY: First results, *Adv. Space Res.*, *34*(4), 780–785.

Smith, L. C., J. Becher, W. B. Fowler, and K. Flemming (1981), Proton-induced noise in Space Telescope digicon, *Proc. SPIE Int. Soc. Opt. Eng.*, *279*, 65–156.

Soller, R., J. M. Nicovich, and P. H. Wine (2001), Temperature-dependent rate coefficients for the reactions of Br ($^2P_{3/2}$), Cl ($^2P_{3/2}$), and O (^3P_J) with $BrONO_2$, *J. Phys. Chem.*, *105*, 1416–1422.

Strong, K., B. M. Joseph, R. Dosanjh, I. C. McDade, C. A. McLinden, J. C. McConnell, J. Stegman, D. P. Murtagh, and E. J. Llewellyn (2002), Retrieval of vertical concentration profiles from OSIRIS UV–visible limb spectra, *Can. J. Phys.*, *80*, 409–434.

Sturges, W. T. (1993), Halocarbons in the Arctic and Antarctic atmosphere, in *The Tropospheric Chemistry of Ozone in the Polar Regions*, edited by H. Niki and K. H. Becker, pp. 117–130, Springer, New York.

Tanzi, C., R. Snel,, O. Hasekamp, and I. Aben (2001), Degradation of observations in the UV of the Global Ozone Monitoring Experiment (GOME), in *IRS 2000: Current Problems in Atmospheric Radiation*, edited by W. L. Smith and Y. M. Timofeyev, pp. 181–184, A. Deepak, Hampton, Va.

Thomason, L. W., L. R. Poole, and T. Deshler (1997), A global climatology of stratospheric aerosol surface area density deduced from Stratospheric Aerosol and Gas Experiment II measurements: 1984 to 1994, *J. Geophys. Res.*, *102*, 8967–8976.

Vandaele, A. C., C. Hermans, P. C. Simon, M. Carleer, R. Colin, S. Fally, M. F. Mérienne, A. Jenouvrier, and B. Coquart (1998), Measurements of NO_2 absorption cross-section from 42000 cm^{-1} to 10000 cm^{-1} (238–1000 nm) at 220 K and 294 K, *J. Quant. Spectrosc. Radiat. Transfer*, *59*, 171–184.

Van Roozendael, M., et al. (2002), Intercomparison of BrO measurements from ERS-2 GOME, ground-based and balloon platforms, *Adv. Space. Res.*, *29*(11), 1661–1666.

von Glasow, R., R. von Kuhlmann, M. G. Lawrence, U. Platt, and P. J. Crutzen (2004), Impact of reactive bromine chemistry in the troposphere, *Atmos. Chem. Phys.*, *4*, 2481–2497.

von Savigny, C., et al. (2003), Stratospheric ozone profiles retrieved from limb scattered sunlight radiance spectra measured by the OSIRIS instrument on the Odin satellite, *Geophys. Res. Lett.*, *30*(14), 1755, doi:10.1029/2002GL016401.

von Savigny, C., A. Rozanov, H. Bovensmann, K.-U. Eichmann, J. W. Kaiser, S. Noël, V. V. Rozanov, B.-M. Sinnhuber, M. Weber, and J. P. Burrows (2005a), The ozone hole break-up in September 2002 as seen by SCIAMACHY on ENVISAT, *J. Atmos. Sci.*, *62*, 721–734.

von Savigny, C., J. W. Kaiser, H. Bovensmann, J. P. Burrows, I. S. McDermid, and T. Leblanc (2005b), Spatial and temporal characterization of SCIAMACHY limb pointing errors during the first three years of the mission, *Atmos. Chem. Phys.*, *5*, 2593–2602.

Wamsley, P. R., et al. (1998), Distribution of halon-1211 in the upper troposphere and lower stratosphere and the 1994 total bromine budget, *J. Geophys. Res.*, *103*, 1513–1526.

Wilmouth, D. M., T. F. Hanisco, N. M. Donahue, and J. G. Anderson (1999), Fourier transform ultraviolet spectroscopy of the $A^2\prod_{3/2} \rightarrow X^2\prod_{3/2}$ transition of BrO, *J. Phys. Chem. A*, *103*, 8935–8945.

World Meteorological Organization (2003), Scientific assessment of ozone depletion, *Global Ozone Res. Monit. Proj. Rep. 47*, Geneva, Switzerland.

Woyke, T., R. Müller, F. Stroh, D. S. McKenna, A. Engel, J. J. Margitan, M. Rex, and K. S. Carslaw (1999), A test of our understanding of the ozone chemistry in the Arctic polar vortex based on in situ measurements of ClO, BrO, and O_3 in the 1994/1995 winter, *J. Geophys. Res.*, *104*, 18,755–18,768.

Wuebbles, D. J., K. O. Patten, M. T. Johnson, and R. Kotamarthi (2001), New methodology for ozone depletion potentials of short-lived compounds: n-Propyl bromide as an example, *J. Geophys. Res.*, *106*, 14,551–14,571.

Yang, X., R. A. Cox, N. J. Warwick, J. A. Pyle, G. D. Carver, F. M. O'Connor, and N. H. Savage (2005), Tropospheric bromine chemistry and its impacts on ozone: A model study, *J. Geophys. Res.*, *110*, D23311, doi:10.1029/2005JD006244.

Yung, Y. L., J. P. Pinto, R. T. Watson, and S. P. Sander (1980), Atmospheric bromine and ozone perturbations in the lower stratosphere, *J. Atmos. Sci.*, *37*, 339–353.

H. Bösch and R. J. Salawitch, Jet Propulsion Laboratory, Pasadena, CA 91109, USA.

K. Chance, T. P. Kurosu, and X. Liu, Harvard-Smithsonian Center for Astrophysics, Cambridge, MA 02138, USA.

M. Dorf and K. Pfeilsticker, Institute of Environmental Physics, University of Heidelberg, D-69117 Heidelberg, Germany.

J. Frerick, European Space Agency/European Space Research and Technology Centre, NL-2200 AG Noordwijk, Netherlands.

F. Goutail and J.-P. Pommereau, Service d'Aéronomie, Centre National de la Recherche Scientifique, F-91371 Verrières-le-Buisson, France.

L. J. Kovalenko, Division of Geological and Planetary Sciences, California Institute of Technology, Pasadena, CA 91125, USA.

C. A. McLinden, Meteorological Service of Canada, Environment Canada, Toronto, ON, Canada M3H 5T4.

C. E. Sioris, Institute of Space and Atmospheric Studies, University of Saskatchewan, Saskatoon, SK, Canada S7N 5E2. (csioris@cfa.harvard.edu)

M. Van Roozendael, Belgian Institute for Space Aeronomy, B-1180 Brussels, Belgium.

C. von Savigny, Institute of Environmental Physics, University of Bremen, D-28359 Bremen, Germany.